



EPJ B

www.epj.org

Condensed Matter
and Complex Systems

Eur. Phys. J. B **68**, 1–21 (2009)

DOI: [10.1140/epjb/e2009-00080-0](https://doi.org/10.1140/epjb/e2009-00080-0)

Topics in the theory of amorphous materials

D.A. Drabold



Topics in the theory of amorphous materials

D.A. Drabold^{1,2,3,a}

¹ Trinity College, Cambridge, CB2 1TQ, UK

² Clare Hall, Herschel Road, Cambridge, CB3 9AL, UK

³ Dept. of Physics and Astronomy, Ohio University, Athens, Ohio 45701, USA

Received 21 January 2009 / Received in final form 8 February 2009

Published online 6 March 2009 – © EDP Sciences, Società Italiana di Fisica, Springer-Verlag 2009

Abstract. In this Colloquium, I describe some current frontiers in the physics of semiconducting amorphous materials and glasses, including a short, but self-contained discussion of techniques for creating computer models, among them the quench from the melt method, the Activation-Relaxation Technique, the decorate and relax method, and the experimentally constrained molecular relaxation scheme. A representative study of an interesting and important glass (amorphous GeSe₃:Ag) is provided. This material is a fast-ion conductor and a serious candidate to replace current FLASH memory. Next, I discuss the effects of topological disorder on electronic states. By computing the decay of the density matrix in real space, and also computing well-localized Wannier functions, we close with a quantitative discussion of Kohn's *Principle of Nearsightedness* in amorphous silicon.

PACS. 61.43.-j Disordered solids – 61.43.Bn Structural modeling: serial-addition models, computer simulation – 61.43.Fs Glasses – 71.23.Cq Amorphous semiconductors, metallic glasses, glasses – 71.23.An Theories and models; localized states – 66.30.Dn Theory of diffusion and ionic conduction in solids – 71.23.-k Electronic structure of disordered solids

1 Introduction

Amorphous materials are among the most important for applications ranging from art to optoelectronics. While our ancestors have been making glass since the Bronze Age (*ca.* 3000 BC), scientists have only started to unravel the structure of this familiar material in the last century, and there is still much work to be done. The applications of amorphous materials are incredibly varied [1,2]. Conventional glass has kept us warmer in winter, decorated cathedrals, been a source of jewelry and adornment since Egyptian times, served as the enclosure for vacuum and cathode-ray tubes, and as the pipeline through which information flows. Amorphous materials like a-Si:H and thin-film oxides are key electronic materials for thin-film transistors, solar photovoltaics and infrared imaging/detection. Diamondlike amorphous C films are standard coatings for drill bits, artificial heart valves and razor blades. Chalcogenide glasses are the basis of current DVD R/W technology, and may emerge as the next generation of computer FLASH memory [3,4].

Amorphous materials are without long range order, but typically have significant *local* chemical and topological order. By this we mean that in most of these systems, the local environment (coordination, nearest-neighbor bond lengths, bond angles with nearest neighbors etc) for a particular species of atom is quite similar

(though not *identical*, as for the case of an ideal crystal). Unlike the case of a crystal, the order rapidly decays with distance: distances of second neighbors are more uncertain than for first neighbors, and so on. The decay of these spatial correlations is an experimental observable via diffraction, and is the first test that a model must pass to merit serious consideration. Glasses are a subset of the broader group of amorphous materials: glasses are made by rapidly quenching a liquid from the melt, resulting in a structure with disorder “frozen in”. Other amorphous materials may be grown by plasma CVD (examples include a-Si:H and a-C:H), and other ways beside, such as ion bombardment.

The disorder in atomic positions leads to emergent phenomena unknown in crystals. The properties of a large collection of atoms with disorder reveal features that are unique, important and useful. The obvious example is that electronic and vibrational states may be localized – confined to a compact volume of space. In crystals, all electronic or vibrational states are extended through space (though not necessarily uniformly) as a trivial consequence of Bloch's theorem. Observables such as the electrical and thermal conductivity are sensitive to localized states, and produce physical properties very different from their crystalline counterparts.

Amorphous materials present a challenge and an opportunity to the condensed matter theorist. There is a zoo of interesting physical processes unique to these systems and important technological applications that could

^a e-mail: drabold@ohio.edu

benefit from materials optimization and basic understanding. Advancement of understanding begins with knowledge of the structure. Thus, the primary challenge to the scientist is to create structural models that faithfully represent the structure. Nowadays, all such studies are undertaken on computers. While it is very easy with current techniques to obtain models, it is difficult to construct models that are entirely adequate – meaning that they agree with what is known of the material: the body of experimental data on the system. Thus, I take an opportunity to discuss the current state of the art for such modeling.

The paper is organized as follows. In Section 2, I begin with a discussion of techniques for modeling amorphous materials. It my intention to make it clear that while there are “standard” methods available, there is tremendous room for development. Since interatomic potentials play a central role, I include a section on the possibilities including empirical potentials and a thumbnail sketch of tight-binding methods and density functional methods (Sect. 3). I divide modeling strategies into two categories, the *Simulation paradigm* (Sect. 4) and the *Information paradigm* (Sect. 5). In Section 6, I describe the Wooten-Weaire-Winer [5] and other specialized methods. In Section 7, I study a chalcogenide glass solid electrolyte material, glassy GeSe₃:Ag. Having focused up to this point on structural aspects of materials, the last part of the paper is devoted to electronic properties (Sect. 8), the nature of the localized to extended transition in amorphous materials, and universal aspects of this transition. I close with a calculation quantifying the locality of a-Si by applying Kohn’s Principle of Nearsightedness [6].

2 Modeling amorphous materials

The first responsibility of a theorist modeling any disordered material is to create a reasonable structural model. Such model building is an example of what is sometimes called an *inverse problem*: given some incomplete (experimental) information about a material, infer its structure. Thus, one can begin with measured pair-correlation functions (or static structure factors) and try to find atomic coordinates reproducing the measurements. The information in the pair distribution function of amorphous materials is inadequate to uniquely specify coordinates in a model, as we discuss below (Sect. 5.1). Indeed, no currently conceivable set of experiments implies a unique model. It *may* be the case that a set of experiments by themselves might *usefully* constrain the coordinates to a representative subspace of all possible models. The need for “reducing the dimension of the subspace” is clear from the work of Stillinger [7], who shows that the number of energy minima scales exponentially with system size.

Because most measured quantities are averaged over macroscopic numbers of atoms, each with a unique environment, the outcome of experiments is usually smooth and rather featureless, and therefore carries limited information. The contrast is to a field like protein crystallography [8], in which exquisite detail is provided by diffraction

data resembling a palisade of δ functions. This information leads to impressive reconstructions of huge *crystal* unit cells. The smooth curves obtained from amorphous materials carry much less information and therefore specificity about microstructure. Another fundamental limitation of the conventional diffraction measurement is that it is sensitive only to pair correlations. An exception to this rule is the so-called Fluctuation Electron Microscopy due to Treacy, Gibson and Voyles [9], which has some sensitivity to three and four body correlations. One should understand diffraction experiments on amorphous materials as providing sum rules which must be satisfied, but are inadequate by themselves to identify a model.

One important case in which experiments imply local information about some atoms is from spectroscopy (electronic, magnetic or optical). For example, electronic defect states in the optical gap are localized and possess well-defined energies. Such information provides a window into the local environment of a tiny fraction of the sites, though it is just such atoms that tend to determine transport and optical properties.

Thus, while we argue that experiments do not adequately constrain atomic positions, any model which is to be believed must reproduce all the experiments available. Obvious as this is, a many papers celebrate agreement with one incomplete measure (a single experiment, typically diffraction) and ignore other experiments. In fairness, it is usually difficult to match all of this information, but it is a goal that we must strive for.

3 Interatomic potentials for disordered materials

3.1 Overview

The capability to accurately compute the total (system) energy and interatomic forces is essential to gauge the credibility of a model amorphous solid. If interatomic forces are available, then it is possible to use this information to relax the model to obtain a structure closer to equilibrium. The interatomic potential and its gradients are such basic tools for the modeler that we include a brief, self-contained introduction to their estimation.

For amorphous materials the interatomic potential $\Phi(\mathbf{R})$ (here \mathbf{R} represents the set of all the atomic coordinates) arises from the chemical bonding between the various constituent atoms. The chemical bond is a spatially non-local entity, the details of which depend sensitively on the local topology (see Sect. 8). Thus, the most reliable approach to modeling Φ is to acknowledge the origin of the complexity (multi-atom forces originating in complicated electronic effects), and start with an attempt to model the electronic structure of the system (either with a tight-binding approach or a more fundamental ab initio method).

Amorphous materials pose a special challenge to any assumed potential, because the disorder implies a wide range of bonding environments. For any empirical potential, there is inevitably a “memory” of the database used

to fit the potential in the first place. This means that the assumed potential will be reliable for structures topologically similar to what was included in the fitting database, but possibly unreliable for topologies that are “new” to the potential. In the interatomic potential lore, the ability of a potential to properly describe a broad range of local bonding environments is called *transferability*.

In the following, I briefly review some of the approaches to approximating Φ .

3.2 Empirical classical potentials

Early potentials were devised by guessing a functional form with free parameters. These parameters were then adjusted to ensure that known properties (bond length, bond angle, melting point, bulk modulus) in reference system(s) (solid, liquid or molecular) were reproduced.

Pair potentials are usually a poor approximation for solids, particularly for covalent systems with directed bonds. The inadequacy of the pair interaction is easily understood for a system like Si or C: if one imagines a pair of bonded Si atoms, it is evident that a third atom placed at a distance comparable to the separation between the first two will affect the strength of the interaction between the initial pair because the presence of the third atom will cause the electronic hybridization to change. Thus, three-body forces are important. The argument can be repeated for a fourth atom interfering with a group of three, *mutatis mutandis*. This depressing *gedanken* experiment can be truncated eventually, but only after many atoms are included (see Sect. 8.4 for a quantitative discussion of locality in amorphous materials). To grapple with this nonlocality, a quantum mechanical calculation of some form is required [10].

Some systems are harder to model than others. Carbon is especially difficult since it can form nearly energetically degenerate tetrahedral sp^3 bonds (as for diamond), and trigonal sp^2 bonds (as for graphite). Thus, it is difficult for a carbon potential to properly differentiate different topologies which are possible in a-C [11]. Silicon is easier to describe because of a strong preference for tetrahedral geometries, a consequence of its tendency to form sp^3 bonds. For either C or Si, it is not difficult to construct a potential which is accurate for a single topology, and small variations about that ideal (as accomplished with a Keating potential [12]). In some ways SiO_2 is easier to handle, since the basic unit of the glass (the crystals, or even the *liquid* [13]) is the $\text{Si}(\text{O}_{1/2})_4$ tetrahedron. The ionicity of silica essentially forbids “wrong” (homopolar) bonds, which is another key constraint which can be built into a reliable SiO_2 potential; no such information is available for elemental Si or C. VanBeest and coworkers [14] have published notably successful potentials that have led to excellent models of g- SiO_2 [15].

3.3 The tight-binding method

Beginning in the seventies and eighties, and thanks especially to the work of Harrison [16], the empirical tight

binding (TB) method grew from a pedagogic mainstay in textbooks into a powerful tool for understanding a great many features of solids. It has been continuously advanced since into a practical tool for computing total energies and forces (and is therefore the heart of many MD simulations).

In the TB approximation, we imagine that the electronic eigenstates can be represented by a linear combination of atomic orbitals: $|\psi_i\rangle = \sum_{\mu} a_{\mu}^i |\mu\rangle$ where μ is a site-orbital index and i indexes the band or state. This method enables the calculation of an approximate one-body Hamiltonian matrix, whose eigenvalues are taken to approximate the allowed electronic energies and the eigenvectors are the states. An interesting feature of TB calculations is that $|\mu\rangle$ are never *explicitly* used. Instead, rules for the distance dependence of the basic matrix elements (such as $s-s$ or $\pi-\pi$, etc.) are devised from a fitting procedure. In the usual implementation of TB calculations, the basis is taken to be orthonormal: $\langle \mu | \nu \rangle = \delta_{\mu\nu}$. Also, most TB Hamiltonians include interactions only with near neighbors and include only two-center contributions. The eigenvectors are filled up to the Fermi level in the usual way. The sum of the occupied eigenvalues is the (attractive) electronic contribution to the total energy [17]. To compute the system (ions + electrons) energy a repulsive interaction must be added to the electronic part. This is obtained from some fitting procedure. TB is the simplest approach enabling an estimate of the many-body forces characteristic of covalently bonded materials.

Transferability is an issue for tight-binding methods, as for other potentials. The simplified form for the Hamiltonian (two-center approximation and assumed orthogonal basis set) are probably most important in this connection. The first TB force calculations were due to Sankey and Allen [18]. The most widely used TB Hamiltonians for force calculations are those of Goodwin-Skinner-Pettifor [19] type. The original [19] was for Si; this was adapted by Xu et al. [20] to carbon systems. The next step in complexity is to use a non-orthogonal Hamiltonian, and really “work out” the matrix elements. In this category is a Hamiltonian whose form is motivated by density functional theory, explicitly using squeezed (spatially confined) atomic orbitals as basis functions [21].

The TB method fills an important niche between empirical potentials, with their serious issues of transferability and ab initio methods with their impressive accuracy, but equally impressive demands on CPU and memory. After the hard work of building a fairly transferable TB Hamiltonian, it is relatively easy to get good performance from massively parallel computers, since virtually all of the computer time is spent in diagonalization. Current high performance computers routinely have parallel libraries available that allow for the efficient use of many processors for diagonalization. Finally, as the TB approach is based conceptually upon a real-space localized representation for the electron states, the method is ideally suited to linear scaling algorithms [22] based on a real-space localized representation for electrons, either with the density matrix or Wannier functions (see Sect. 8).

Colombo [23] and Lewis and Mousseau [24] have reviewed the use of TB for disordered systems. In addition, Colombo has made a convenient public domain TB simulation code available for download [25].

3.4 Ab initio methods

From a fundamental point of view, the complexity of electronic structure and force calculations arises from the many-body nature of the interactions between the electrons. Currently, it would seem that direct attacks on the many-electron problem is too difficult to have direct impact on amorphous systems, requiring as they do a large number of atoms to provide a model worth investigating. Thus, all the successful electronic structure calculations on amorphous insulators have involved some kind of mapping of the many-body problem into an effective one-electron problem. Historically, the Hartree [26] and Hartree-Fock [27] approximations were the first success in this direction; descendants of these methods are widely used today, particularly in quantum chemistry. Tight-binding captures some of the many-body effects, albeit in an empirical fashion.

Because of the mass difference between the electrons and nuclei, it is possible to decouple the nuclear and electronic degrees of freedom with the adiabatic or Born-Oppenheimer approximation [28,29], in which the electrons are assumed to respond instantly to motions of the ions (the electrons are taken to be in their ground state for all instantaneous ionic conformations). In addition, the nuclei are treated as classical particles which move in a potential determined by the electrons in their ground state, computed for the instantaneous ionic coordinates.

Virtually all ab initio calculations are based on “density functional” methods. The conceptual basis of density functional theory is to work with the electronic charge density rather than the many-particle wave functions¹. The idea extends back to Thomas and Fermi [30], and the charge density emerges naturally as a key quantity in Hartree and Hartree-Fock calculations. The logic justifying the elevation of the charge density to primacy in electronic structure calculations is due to the work of Kohn, Hohenberg and Sham [31]. One of the most appealing features of DFT is that it is, in principle, an exact theory.

The following statements are the basis of zero-temperature DFT:

(1) The ground state energy of a many electron system is a functional of the electron density $\rho(\mathbf{x})$:

$$E[\rho] = \int d^3x V(\mathbf{x})\rho(\mathbf{x}) + F[\rho], \quad (1)$$

where V is an external potential (due for example to interaction with ions, external fields, e.g., *not* with electrons),

¹ Kohn gives a fascinating argument that it does not make sense, *even in principle* to try to compute the many-electron wave function systems with more than *ca.* 100 electrons [6].

and $F[\rho]$ is a *universal* functional of the density. The trouble is that $F[\rho]$ is not exactly known, though there is continuing work to determine it. The practical utility of this result stems from:

(2) The functional $E[\rho]$ is minimized by the true ground state density.

It remains to estimate $F[\rho]$, which in conjunction with the variational principle (2), enables calculations on materials. To estimate $F[\rho]$, the usual procedure is to note that we know some of the major contributions to $F[\rho]$, and decompose the functional in the form:

$$F[\rho] = e^2/2 \int d^3x d^3x' \rho(\mathbf{x})\rho(\mathbf{x}')/|\mathbf{x} - \mathbf{x}'| + T_{ni}(\rho) + E_{xc}(\rho). \quad (2)$$

Here, the integral is just the electrostatic (Hartree) interaction of the electrons, T_{ni} is the kinetic energy of a *noninteracting* electron gas of density ρ , and $E_{xc}(\rho)$ is yet another unknown functional, called the “exchange-correlation” functional, which includes nonclassical effects of the interacting electrons. Equation (2) is difficult to evaluate directly in terms of ρ (because of the term T_{ni}). Thus, one introduces single-electron orbitals $|\psi_i\rangle$, for which $T_{ni} = \sum_{i \text{ occ}} \langle \psi_i | -\hbar^2/2m \nabla^2 | \psi_i \rangle$, and $\rho = \sum_{i \text{ occ}} |\psi_i(\mathbf{x})|^2$ is the charge density of the physically relevant *interacting* system. The value of this decomposition is that $E_{xc}(\rho)$ is a smooth and slowly-varying functional of the density: we have included the most difficult and rapidly varying parts of F in T_{ni} and the Hartree integral, as can be seen from essentially exact many-body calculations on the homogeneous electron gas [33]. The Hartree and non-interacting kinetic energy terms are easy to compute and if one invokes the “local density approximation” (taking the electron density to be *locally* uniform), and using the results for the homogeneous electron gas, functional (Eq. (2)) is fully specified.

With noninteracting orbitals $|\psi_i\rangle$,

$$\rho(\mathbf{x}) = 2 \sum_{i \text{ occ}} |\psi_i|^2, \quad (3)$$

then the minimum principle plus the condition that $\langle \psi_i | \psi_j \rangle = \delta_{ij}$ can be translated into an eigenvalue problem (the celebrated Kohn-Sham equation) for the $|\psi_i\rangle$:

$$\{-\hbar^2 \nabla^2 / 2m + V_{\text{eff}}[\rho(\mathbf{x})]\} |\psi_i\rangle = \epsilon_i |\psi_i\rangle, \quad (4)$$

where the effective (density) dependent potential V_{eff} (in practical calculations orbital dependent) is:

$$V_{\text{eff}}[\rho(\mathbf{x})] = V(\mathbf{x}) + e^2 \int d^3x' \rho(\mathbf{x}')/|\mathbf{x} - \mathbf{x}'| + \delta \epsilon_{xc}/\delta \rho. \quad (5)$$

In this equation ϵ_{xc} is the parameterized exchange-correlation energy density from the homogeneous electron gas. The quantities to be considered as physical in local density functional calculations are: the total energy (electronic or system), the ground state electronic charge density $\rho(\mathbf{x})$, and related ground state properties like the forces. In particular, it is tempting to interpret the $|\psi_i\rangle$ and ϵ_i as genuine electronic eigenstates and energies (and

indeed this can often be useful); but such identifications are not rigorous [34]. Note that the starting point of density functional theory was to depart from the use of orbitals and formulate the electronic structure problem rigorously in terms of the electron density ρ ; yet a practical implementation (which enables an accurate estimate of the electronic kinetic energy) led us immediately back to orbitals! This illustrates why it would be very worthwhile to know $F(\rho)$, or at least the kinetic energy functional since we would then have a theory with a structure close to Thomas-Fermi [30] form and would therefore be able to seek *one* function ρ rather than the cumbersome collection of orthonormal $|\psi_i\rangle$.

The usual implementation of LDA leads to a nonlinear set of coupled integrodifferential equations. The origin of this nonlinearity is that V_{eff} in the Schrödinger-like (Eq. (4)) is ρ -dependent, which in turn depends on the eigenvectors $|\psi_i\rangle$, which in turn depend on V_{eff} and so on. This nonlinearity is dealt with in the usual way “iterating to self consistency”, an expensive inner loop on an already challenging computational task. The development of practical density functional codes is a vast undertaking. Several “standard” codes are now in general use. Among these are SIESTA [35] and FIREBALL [36] which employ local basis sets and VASP [37], CASTEP [38], CPMD [39], quantum espresso [40] and ABINIT [41] which use a plane wave representation. Each of these codes has been immensely successful, and all have contributed to the theory of disordered systems.

The discovery and practical development of density functional methods has proven to be a transformational step in modeling amorphous materials but also for solid state and molecular physics generally. The reason for this bold claim is that the methodology offers genuinely *predictive* capability for a wide variety of materials. It has enabled the construction of structural models of previously poorly understood materials, and also allows many direct connections between theory and experiment – density functional calculations routinely provide structural, vibrational, electronic, optical and other information that may be compared confidently with experiments.

4 Simulation paradigm

4.1 Molecular dynamics simulation

The idea of molecular dynamics (MD) is implicit to a Newtonian view of the world. If we possess the coordinates and velocities of a collection of particles and we know the interatomic force, then Newton’s second law deterministically specifies the time evolution of the system for all later times. Classical statistical mechanics is concerned in part with macroscopic prediction derived from the collective properties of large systems obeying classical mechanics.

So far as I can tell, the first MD simulation was performed by an astronomer without a computer. During the second World War, Erik Holmberg [42], was concerned with modeling energy transfer between colliding galaxies.

His idea was to exploit the identical radial ($1/r^2$) dependence of the light intensity and the gravitational force, to enable simulations based upon an “optical analog” of the gravitational interaction. Holmberg constructed a remarkably ingenious apparatus in which two groups of 37 lamps each (each lamp representing a star, each group representing a galaxy) interacted optically, and the light intensity at each lamp (“star”) was measured with photocells. Since the intensity² was proportional to the interstellar forces, the time evolution of a galactic collision could then be simulated, and Holmberg was able to see spiral arms and learn something about capture probability. This study was the ancestor of all MD simulations since [43].

For disordered solids, the simulation paradigm is realized by attempting to model the transition from a liquid to a disordered solid on a computer. One begins by forming a well-equilibrated computer model of the liquid [44], and then applies some form of dissipative dynamics to “cool” the liquid through something analogous to the glass transition. We name this the “melt-quench” method.

Empirically, there have been successes for the melt-quench method, as demonstrated for silica [45] and certain chalcogenide glasses [46,47]. Advocates of the method assert that it is unbiased (not forcing the system toward any a priori preferred result). This is not entirely true, since the method is clearly biased to incorporate too much liquid character into the solid state.

It is reasonable to conjecture that melt-quench should work when (1) the structure of the liquid is essentially similar to the structure of the glass, (meaning that similar fundamental units or building blocks are present in both) and (2) the ordering is quite local (which amounts to saying that the building blocks from which the glass (and liquid) is composed are quite small). The failure of the method to produce realistic models (that is, with a small concentration of coordination defects) of Si is probably connected to the fact that the liquid is \sim 6-fold coordinated and a metal [48], whereas the amorphous phase is a tetrahedral insulator with a concentration of non four-fold atoms less than 0.01%. Also, experimentally, a-Si is not a glass. Rapidly quenching the liquid does not produce a-Si, which is formed with ion bombardment or chemical vapor deposition techniques. For a recent analysis of the point, see reference [49]. In g-GeSe₂, a classic stoichiometric chalcogenide glass, we have seen that quench from the melt does a respectable job, though it leaves signatures of excessive liquid-like character in the static structure factor [46,47]. Because it is such a conceptually straightforward scheme for making models, it is always the first technique to try on *terra incognita*.

4.2 Landscape methods; activation-relaxation technique

Away from the melting temperature, many materials explore a sequence of metastable states separated by energy

² Holmberg used selenium photocells to measure the light intensity. We may hope that they were amorphous.

barriers much larger than $k_B T$, the typical excitation energy scale at the atomic level. For long periods of time, the configuration vibrates around a given metastable state, then, due to rare energy fluctuations, it will find enough energy to jump over a barrier and move to a new metastable state. The dynamics of these materials is therefore dominated by the rates controlling the jumps from one metastable state to another.

It is possible to do better by directly focusing on the rare events. To a first approximation, these are fully determined by the activation energy, i.e. the energy needed to bring a configuration from a local configurational minimum to a nearby saddle point. A low temperature characterization of the dynamical properties of a disorder system can therefore be made by reducing the configuration energy landscape to a network of local minima connected by paths going through first order saddle points. Recently, Barkema and Mousseau have proposed such a procedure, the activation-relaxation technique (ART), which provides a local prescription for moving from one minimum to another one with a trajectory passing by a shared saddle-point (event) [50].

The advantage of ART is that it defines moves directly in the configurational energy landscape, which really controls the dynamics, instead of trying to map events into complicated real-space moves. ART is independent of the details of the interaction potential and the specificity of a given material and requires only a local and continuous description of the energy landscape.

An event in ART is defined as a move from a local energy minimum $\mathbf{M}^{(0)} \equiv \mathbf{R}^{(0)}$ to another nearby minimum $\mathbf{M}^{(1)} \equiv \mathbf{R}_1^{(1)}$ following a two-step process mimicking a physical activated processes:

- (i) the **activation** during which a configuration is pushed from a local minimum to a nearby saddle-point;
- (ii) the **relaxation** which brings the configuration from this saddle-point to a new local minimum.

The details of how the saddle point is reached, and other technical points concerning the implementation may be found in the literature [50].

ART has already been applied with success to a series of static problems in metallic glasses, *a*-Si [50] and *a*-GaAs [52,53]. A slightly different version of the algorithm was also developed independently by Doye and Wales and applied to map the full energy landscape of a 13-atom Lennard-Jones cluster [54]. In reference [55], ART was applied to Lennard-Jones clusters and it was demonstrated that ART converges on saddle points using a Lanczos [56] scheme.

Because it necessitates only the calculation of the force, ART is scalable with the size of the systems studied. In general, about a 1000 force evaluations per event are necessary. This means that ART will be useful for activated processes with barriers significantly larger than the temperature of the material studied. In this case, though, it provides a unique tool for the description of rare events such as diffusion and relaxation mechanisms in disordered materials.

5 Information paradigm

5.1 Reverse Monte Carlo

A different approach to structural modeling begins with the manifestly sensible principle that a model should agree with experiments. So, rather than making a model by imperfectly mimicking the process of glass formation, the idea is to construct the model using known experimental facts. The method appears to have been first adopted by Kaplow and co-workers [57] as a means to make atomistic models of vitreous Se consistent with their X-Ray diffraction measurements. The idea was greatly extended and developed by McGreevy and Puzstai [58] who named it the Reverse Monte Carlo (RMC) method. A popular recent outgrowth is the EPSR [59] method for dealing with partial structure factors.

The MD method is a direct approach: a simulation procedure is adopted that results in a structural model that is then compared to experiment. RMC proceeds in the opposite direction, and produces models directly from information implied by experiment. To implement this, the goal is find a set of coordinates that minimize the difference between model and experiment:

$$\chi^2(\mathbf{R}) = \sum \eta_i \{F_E(Q_i) - F_m(\mathbf{R}, Q_i)\}^2 \quad (6)$$

where the sum runs over all data points Q_i , $F_E(Q_i)$ is the value of an experimental observable at that point, $F_m(\mathbf{R}, Q_i)$ is the value of the observable given by the model at the data point and for a given collection of atomic coordinates \mathbf{R} . The η are non-negative weights for the data points, possibly associated with experimental error. By construction $\chi^2 \geq 0$, with equality if and only if the model and experiment exactly coincide at all the data points Q_i . We face an optimization problem of finding a set of \mathbf{R} satisfying $\chi^2 = \min$. Evidently χ^2 is a measure of goodness of fit (between experiment and model), as is well known from elementary error analysis. This is the simplest version of RMC: the method has been generalized in many ways, to include joint analysis of multiple experimental data sets, and the inclusion of constraints (requiring specified coordination of atoms, for example). Note that the method has the attractive feature that *no interatomic potential is required*.

This approach is much like a structural refinement method, in which atomic positions are tuned to be consistent with scattering or spectroscopy data. For amorphous materials, the data are smooth from structural averaging, and there is no unit cell, as in a crystal. The data constrain the structural models for amorphous materials, but far less rigorously than for a case like protein crystallography. Thus, in analogy with the problem of minimizing the potential energy in a MD quench, RMC faces the problem of too many minima (the possibility of a minimization procedure getting stuck at a configuration that makes $\chi^2 = \min$, but for a poor fit). This can usually be overcome with a Monte Carlo minimization [61]. More seriously, many highly discrepant configurations produce a

satisfactorily small χ^2 . This means that in practice a further analysis is required: since many different models fit experiment (by construction), the “structural degeneracy” must be broken by some criterion external to the experiment, such as expectations of chemical order, coordination etc. Current implementations of the RMC method recognize this, and a very useful C++ code has been released [60].

The RMC method is particularly useful when we do not possess interatomic potentials, or the energy is prohibitively expensive to compute. It is also a flexible tool, allowing one to compare the structural information in one experiment relative to another, and even to determine the structural consequences of one part of a data set relative to another. It is also an ideal way to create a first model (that might, for example, locally constrain desirable chemical and topological order) that may be analyzed or further relaxed by other methods.

5.2 Including Φ

Consistent with the information-based logic of the preceding section, it is desirable to include all the information available in the process of model construction. This should include experimental information and information inherent to accurate interatomic interactions. The intuitive means to accomplish this is to add a term to the RMC function:

$$\xi(\mathbf{R}) = \chi^2(\mathbf{R}) + \Lambda\Phi(\mathbf{R}), \quad (7)$$

where $\Lambda > 0$. Then one minimizes the generalized penalty function ξ , finding a configuration satisfying:

$$\partial\xi/\partial\mathbf{R}_\alpha = 0; \alpha = 1, 2, \dots, N. \quad (8)$$

This has been carried out for models of amorphous carbon [62] with an empirical potential and a Monte Carlo minimization of ξ , and before that, for biomolecules [63]. For an ab initio Hamiltonian this is expensive, since Monte Carlo minimization of equation (7) requires a very large number of energy/force calls. Also, the parameter Λ is essentially a weight factor indicating the relative importance of experiment (first term) and energy (second term). Within this picture, there is no well-justified way to specify Λ .

An alternative, *Experimentally Constrained Molecular Relaxation* (ECMR), employs a self-consistent iteration scheme: (1) starting with an initial generic conformation \mathbf{R}_1 , minimize equation (7) to get \mathbf{R}_2 ; (2) steepest-descent quench \mathbf{R}_2 with an *ab initio* method to get \mathbf{R}_3 ; (3) subject the resulting conformation to another RMC run (minimize again); repeat steps (2) and (3) until both the force field relaxed model and RMC models no longer change with further iteration. For the RMC component of the iteration, one makes the conventional choice of using Monte Carlo for the minimization. This is easily implemented and does not require gradients (and thus allows the use of non-analytic terms in Eq. (7), if desired). This method

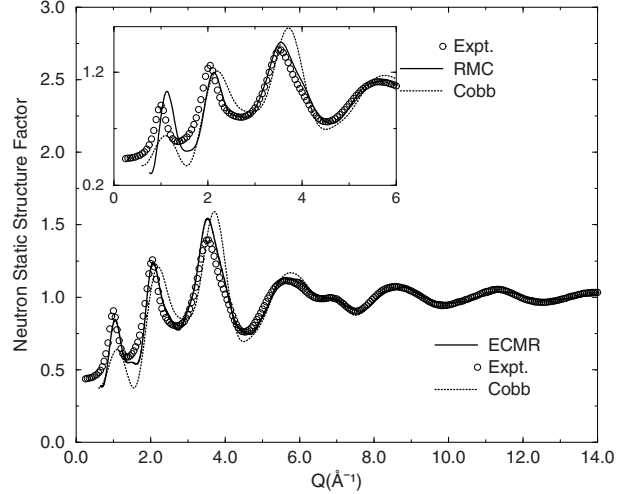


Fig. 1. Neutron structure factor of g-GeSe₂: experiment, 647-atom ECMR model and 216-atom quench from the melt model (designated “Cobb” [47]). Note the improved agreement on the first sharp diffraction peak (near $Q = 1 \text{ \AA}^{-1}$) for the experimentally constrained molecular relaxation calculation. From [65].

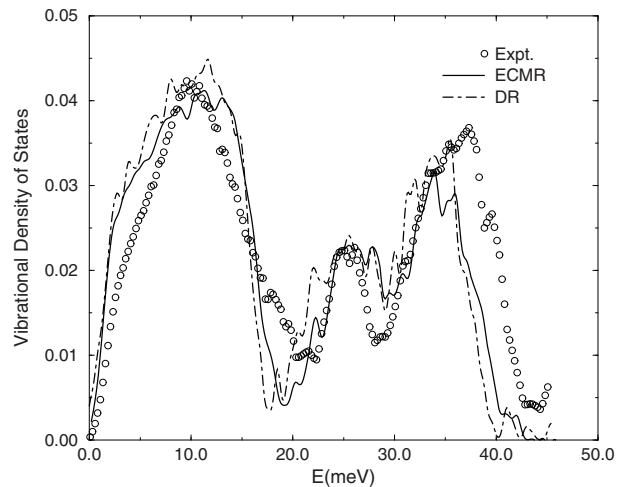


Fig. 2. Vibrational density of state of g-GeSe₂: experiment [66], decorate and relax [76] and ECMR models [65]. Note the middle band, associated with a tetrahedral breathing mode. From [65].

has produced satisfactory results on g-GeSe₂ [65], the first application of such a technique on a network glass. The results for this glass are shown in Figure 1. In Figure 2, the vibrational power spectrum is presented, with the characteristic “three hump” structure; the middle band being associated with the tetrahedral breathing modes [66].

ECMR has also been applied to a-Si:H [67].

5.3 A Bayesian approach

An appealing approach that has recently been applied to biomolecules might establish these methods on a more rigorous basis. Bayesian probability theory [68] offers a rigorous and fundamental approach to the Model Selection

Problem, which for our purposes can be stated as: *given information (experimental data and possibly other a priori information), what model best describes this state of knowledge?*

We reproduce the argument here in a simplified form, and suggest that the reader should read the original papers [70]. If \mathbf{R} denotes a structural model (a set of coordinates) then the probability that \mathbf{R} is valid given experimental data D is provided by Bayes theorem:

$$P(\mathbf{R}|D) \propto P(D|\mathbf{R})P(\mathbf{R}). \quad (9)$$

This statement relates the probability that a model describes the data to a product of probabilities: the probability that the data is reproduced from the model (the likelihood) times the a priori probability that the model is valid (e.g., based upon considerations other than the data D). A quantitative evaluation of $P(\mathbf{R}|D)$ is valuable, since it allows one to quantify the credibility of different models, and provides a measure of quality on the space of structural models, which we may then seek to maximize. The sharpness of the maximum is a measure of confidence in the model (or information content in the data). With some additional assumptions, Habeck et al. [70] argue that the prior $P(\mathbf{R}) \propto \exp(-\Phi(\mathbf{R})/kT)$, and $P(D|\mathbf{R})$ is related to χ^2 leading to the conclusion that maximizing $P(\mathbf{R}|D)$ is achieved by minimizing the functional:

$$\xi_B(\mathbf{R}) = n/2 \log \chi^2(\mathbf{R}) + \Phi(\mathbf{R})/kT \quad (10)$$

where n is the number of data points, k is Boltzmanns constant and T is the temperature. Minimizing equation (10) modifies the model (changes the coordinates) to minimize the energy while also reproducing experiment. Indeed, the gradient of the first term is essentially a fictitious force that pushes the system toward agreement with experiment. The form (Eq. (10)) quantifies the relative importance of the data and the potential energy, and clarifies the role of the temperature.

6 Specialized methods

6.1 Wooten-Weaire-Winer

For the peculiar case of tetrahedral amorphous insulators a-Si and a-Ge, the finest models are made with the “WWW” technique, due to Wooten, Winer, and Weaire [5]. This technique is essentially a Monte Carlo modeling approach with inspired moves. In the original version, one starts with a perfect diamond structure, and then adopts the WWW bond transposition or bond switch. For a bonded pair of atoms BC a pair of nearest neighbors A and D is chosen, so that A is the neighbor of B and not the neighbor of C, and D is the neighbor of C and not the neighbor of B. Then bonds AB and CD are broken (deleted from the bond lists for atoms B and C) and new bonds AC and BD are created (added to the appropriate bond lists), i.e. atoms B and C exchange neighbors. This procedure effectively introduces five- and sevenfold rings –

which are a characteristic structural feature of the CRN – *while preserving four-fold coordination*. The method was extended to binary glasses by Mousseau and Barkema [71].

Monte Carlo moves are accepted in Metropolis [61] fashion with Keating springs as the interatomic potential. In practice, the method is not trivial to implement, as one needs to introduce sufficient disorder (so that the system does not return to a crystalline state) and a proper simulated annealing scheme to produce an optimal network. Mousseau and Barkema [72] have shown that it is not necessary to start with diamond – a completely random configuration leads ultimately to topologically identical networks as those obtained from the randomized crystal. Carefully devised WWW networks are in remarkable agreement with experiment on structure, electronic structure and dynamics. The method is successful for two reasons: (1) the moves identified by WWW are in fact quite physical, as shown by the Activation Relaxation Technique (ART) [72] (Sect. 4.2), and (2) the method compels the system to retain four coordination, and indeed to force bond angles close to be near the tetrahedral angle (through the bond angle springs in the potential). This second condition amounts to constraining the optimization of the network to satisfy a priori information (which can be inferred from optical and other measurements). In the spirit of my “paradigm” subdivision of methods, WWW involves aspects of simulation (Metropolis annealing) and information (imposition of constraints on network topology). The method is flexible, and has been used for heterogeneous phases of a-Si with crystalline inclusions [73] (these appear to be important for photovoltaic applications).

6.2 Decorate and relax

In this section, I present an approach for modeling certain binary glasses. We begin with a WWW model of a-Si. This model is strictly four-coordinated, and has bond angles tightly centered on the tetrahedral angle. We decorated the Si–Si bonds with a bond-centered atom from column VI, and rescaled the coordinates to the experimental density of the glass desired (eg, SiO_2 , GeSe_2 , etc.). Then we relax the resulting model with an ab initio method (Sect. 3.4). We name this scheme “decorate and relax” [76]. It is somewhat surprising that the resulting models are often very realistic (compared to experiments). Such models are easy to generate, and preliminary work with Chubynsky and Thorpe suggests that the approach may be extended to off-stoichiometric compositions. Vink and Barkema have also explored similar methods in silica [77]. The concept of bond-decoration certainly predates our work [74], though ab initio relaxation seems to begin with reference [76].

Here, I review 192 and 648-atom Decorate and Relax models of g- SiO_2 . By taking the Fourier transform of the pair-correlation function we compute the neutron static structure factor $S_N(Q)$, which may be directly compared to experiments. The structure factor of these models, along with experiment is plotted in Figure 3. The

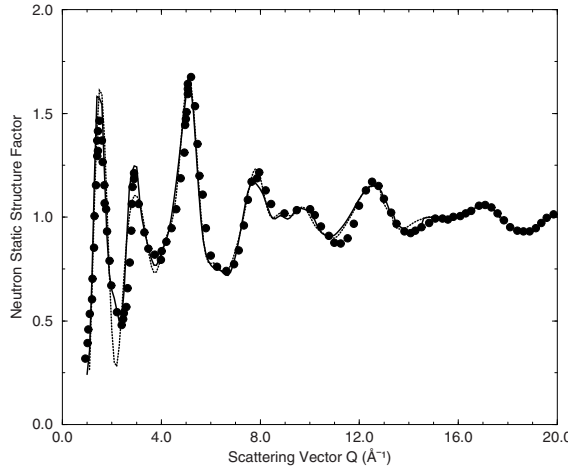


Fig. 3. Calculated total neutron structure factor $S(Q)$ of glassy SiO_2 : dashed lines are for 192-atom model and solid lines are for 648-atom model compared to experimental data [79] (filled circles). We used scattering lengths of $b_{\text{Si}} = 4.149$ and $b_{\text{O}} = 5.803$ fm. From [76].

discrepancy between the 192 and the 648-atom models arises from finite size effects, since the same method was used to generate both models. It is of some interest that the only substantial difference between the 192 and 648 atom models was near 2.0 \AA^{-1} in the minimum after the first diffraction peak. The only remaining discrepancy between theory and experiment appears near 12 \AA^{-1} , and is similar for both models (and so is not due to a finite-size effect).

Another measure of the credibility of any amorphous silica model is the distribution of the O–Si–O and Si–O–Si bond angles in the network. The FWHM of the former distribution is 9° , and of the latter 25° . These numbers are in reasonable agreement with experiments and excellent models made with empirical potentials, and the width of the Si–O–Si distribution is near available experiments [78]. The distribution of bond angles for the models are give in Figure 4.

Decorate and Relax is a simple idea that spares us from the expensive melt-quench technique. The scheme is faster than the traditional methods (at least 10 times faster for a given interatomic interaction). We have seen that the scheme produces a satisfactory *ab initio* model of amorphous silica involving a reasonable number of atoms (648) and accurate forces (from SIESTA [35]).

6.3 Building blocks [80]

We have emphasized the limitations of quench from the melt methods. The prime deficiency is one of *time scales* – the method seems to work if the liquid that is being quenched is topologically akin to the glass. One can understand this situation as one in which there are fundamental structural units, call them *building blocks* (BB) that exist

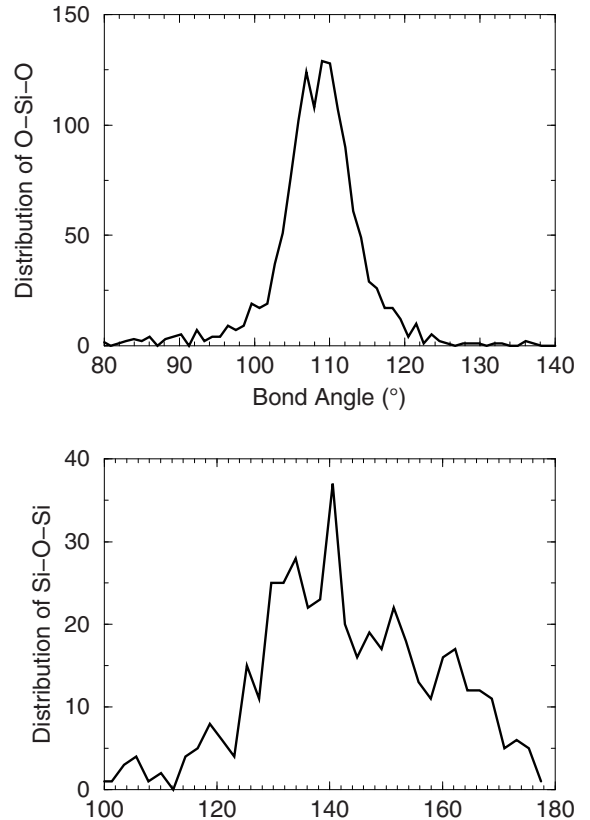


Fig. 4. Bond angle distributions for decorate and relax model of g-SiO_2 . Top: O–Si–O angle; bottom: Si–O–Si. From [76].

in both the liquid and the glass³. If the BBs are simple, such as Si–O tetrahedra, it is not difficult to equilibrate the liquid long enough to produce these. If the BBs of the liquid and glass are different, or if the BBs are very complex, it is likely that melt-quench approaches will be foiled by the limitation of short times. For a general multinary glass, it is likely that the BBs will be complex.

Thus, we have tried to grapple directly with the question of determining energetically reasonable BBs. The idea is to start with a small supercell with enough atoms present to reflect the composition (so that the small cell has the same chemical composition as the glass). Then, we do an extended annealing on the cell to find a minimum energy conformation. The resulting structure forms a crystal with an energetically preferred topology and chemical order. Since the cell is small, we can thoroughly explore the energy minima to find the best candidate BB. While there is no fundamental justification for it, we have so far used only cubic cells for this purpose. Once the preferred small cell is found, we stack several such cells together, melt them (by construction, they have the right stoichiometry), and then we quench the resulting liquid.

We illustrate the static structure factor for a 200-atom model of the ternary glass $\text{Ge}_2\text{As}_4\text{Se}_4$, along with a comparison to experiment in Figure 5 [81]. This model also

³ Of course this is only an assumption. It is conceivable that there are cases in which the BBs do not exist.

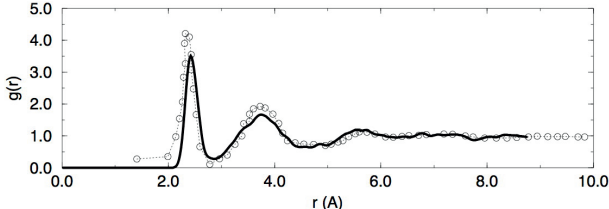


Fig. 5. Radial distribution function for $\text{Ge}_2\text{As}_4\text{Se}_4$ glass, made using the building block method (see text). Experiment [81], open circles, model solid line. From [80].

produced a state-free optical gap of about 0.8 eV [80]. By contrast, a calculation with the same Hamiltonian (FIREBALL [36]) based on the melt-quench approach was completely unsatisfactory, with essentially no optical gap, and an unsatisfactory structure factor. A curious feature of the BB model is that it has limited respect for Mott's 8- N rule [2], as Ge and Se is mostly *three-fold* rather than four fold and two fold. Interestingly, As is almost perfectly three-fold as Mott would predict. The a priori expectation would be that this material should satisfy the 8- N rule, but this is not certain, since, for example, boron regularly violates the rule in a-Si [82]. More work is needed to draw firm conclusions on the BB method, but preliminary signs show some promise.

7 Example: study of a solid electrolyte

Chalcogenide glasses (glasses involving column VI species S, Se or Te) have long held interest for applications, and probably the example of greatest ubiquity is the ternary telluride material used for phase-change optical memory: “Digital Versatile Disks”. Chalcogenide glasses are employed for applications requiring IR-transparent optical windows. The “optomechanical effect [83]” in arsenic sulfide glasses is the only known mechanical manifestation of the polarization of light.

Materials with high ionic conductivity and high electrical resistivity are designated *solid electrolytes*. These materials are used as solid-state batteries and chemical sensors [1]. The best-known example is the lithium “button battery”. Flexible, polymer-based solid electrolytes have even been proposed for automotive (electric car) applications [84]. Chalcogenide glasses in a wide range of compositions become fast ionic conductors with the addition of sufficient quantities of Ag or certain other metals. The Ag^+ ions assume a variety of different coordination patterns in the glassy host with tiny energy differences, and this is the basic reason why Ag^+ is mobile. From a materials point of view it is interesting that an amorphous material should allow rapid motion of a transition metal ion through the network, and a great deal of energy has been devoted to understanding this phenomenon. Such diffusive processes in glasses have been studied for decades with a variety of experimental methods. There have been several approaches to modeling diffusive behavior.

Silver doped chalcogenide glasses are usually made by photodiffusion (shining light of a suitable (UV) wave-

length on a thin Ag layer deposited on the glass surface). Kawaguchi, Maruno and Elliott [85] have studied various Ag/Ge/Se (and analogous sulfide) films, and explored photo-induced surface deposition (in which light induces segregation of small Ag particles at the surface). They also discussed the structure of Ag rich films and discuss phase separation and showed that the maximum Ag concentration was about 40% for amorphous GeSe films. The photodiffusion depends on several external factors including light intensity, wavelength, temperature, pressure, and external electric fields.

Recently, Kawasaki et al. [86] explored the composition dependence of the ionic conductivity in $\text{Ag}_x(\text{GeSe}_3)_{1-x}$ glasses and found a maximum conductivity near $x = 0.3$. Iyetomi, Vashishta and Kalia [87] used MD with empirical potentials to make models for $\text{Ag}_4\text{Ge}_3\text{Se}_9$, and observed a tendency toward Ag phase separation consistent with the neutron diffraction data of Moss and Price [88]. Their interatomic interaction is simple, physically transparent, and appears to capture significant aspects of the material, especially the important tendency of Ag to phase separate. In different glasses, such as Li_2SiO_3 , a novel time series analysis method, the “singular spectrum method” has been employed with empirical potential MD simulations to detail Li^+ motion [89].

In heavily Ag-alloyed glasses (of order 50% Ag), there is another fascinating effect: photodeposition [90]. Here, shining light on the “virgin” surface causes Ag metal to appear. These surface Ag clusters are negatively charged. Lithography can then be used to control the surface properties. For optical recording the best materials are As-based glasses, but the effect is also strong in the GeSe system [91]. These effects occur only for an amorphous host. Recently, it was shown that related glasses are phase separated into a “backbone” phase and a Ag-rich phase [92]. It is quite possible that Ag segregates into Ag_2Se regions for the glasses we model here.

The solid electrolyte memory device of Axon Technologies Corp.⁴ is schematically represented in Figure 6. Application of the bias shown creates electro-deposition of Ag metal starting at the cathode, and the filament grows to reach the anode at which point there is metallic conduction through the cell and a commensurately low resistance. Bias voltages are low (of order 0.25 V). Because the Ag ions diffuse quickly, the switching can be rapid (with a 10 nm bridgeable path switch time is estimated to be less than 10 ns) [93]. For a TEM study of these processes in thin films, see the work of Romero and co-workers [94]. A related device, based upon Ag_2S , has been explored by Terabe and colleagues [95].

While the essential operation of the cell is understood, there is limited microscopic understanding of the ion dynamics in an electric field, the role of the amorphous network, the electro-deposition process and associated chemistry, or the reverse biased case, which injects ions. Despite serious (and successful) experimental efforts to optimize the chalcogenide host for ion mobility, simulation and modeling may further improve upon

⁴ US Patent 5,761,115, and many others.

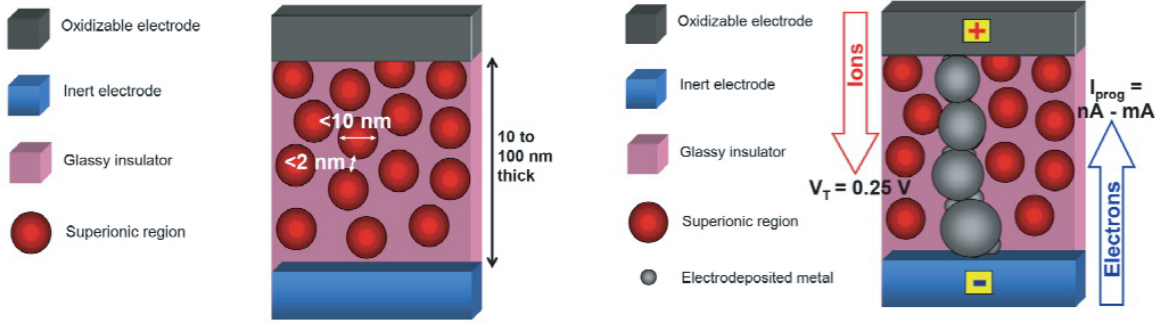


Fig. 6. Schematic representation of Programmable Metallization Cell [93]. Left: initial high resistance state (Ag exists in the form of ions); Right: the cell is biased to grow metallic Ag filaments between cathode (bottom electrode) and oxidizable (Ag) anode (top). The resistance is nearly zero, because of the metallic filament. *Figure courtesy of Kozicki and Mitkova, Arizona State University and Axon Technologies Corp.*

the composition as the atomistics of the process are elucidated.

7.1 Model formation

The models of the silver chalcogenide material were generated using the melt quenching method [96] with the efficient local basis density functional code FIREBALL designed by Sankey, Lewis and coworkers [36]. We randomly placed atoms in a cubic supercell according to the correct stoichiometry [for $(\text{GeSe}_3)_{0.90}\text{Ag}_{0.10}$ 54 germanium atoms, 162 selenium atoms and 24 silver atoms; for $(\text{GeSe}_3)_{0.85}\text{Ag}_{0.15}$ 51 germanium atoms, 153 selenium atoms and 36 silver atoms]. The size of the cubic cells was chosen to make the density of these glasses close to experimental data. The box size of the 240 atom supercell of $(\text{GeSe}_3)_{0.90}\text{Ag}_{0.10}$ and $(\text{GeSe}_3)_{0.85}\text{Ag}_{0.15}$ are respectively 18.601 Å and 18.656 Å with corresponding density 4.98 g/cm³ and 5.03 g/cm³ [98]. The structures were annealed and we obtained well-thermalized melts at 4800 K. We took three steps to cool down the cells. First, the cells were equilibrated and cooled to 1100 K for 3 ps; then they were slowly cooled to 300 K for approximately 5 ps. As final step, the cells were steepest descent quenched to 0 K with forces smaller in magnitude than 0.02 eV/Å. All calculations were performed at constant volume using the Γ point to sample the Brillouin zone in order to compute energies and forces.

7.2 Structure

Figure 7 shows the calculated static structure factors for $(\text{GeSe}_3)_{0.90}\text{Ag}_{0.10}$ and $(\text{GeSe}_3)_{0.85}\text{Ag}_{0.15}$ and the comparison with the experimental data from reference [98]. A feature of interest seen in many glasses is the so called “first sharp diffraction peak” (FSDP [1]) exhibited in both models at about 1.07 Å⁻¹. In this system, for both theory and experiment, the FSDP is more like an oxymoronic “First sharp diffraction shoulder”. Piarristeguy et al. [98] show that this peak varies as a function of Ag content. As Ag concentration increases, the FSDP intensity decreases.

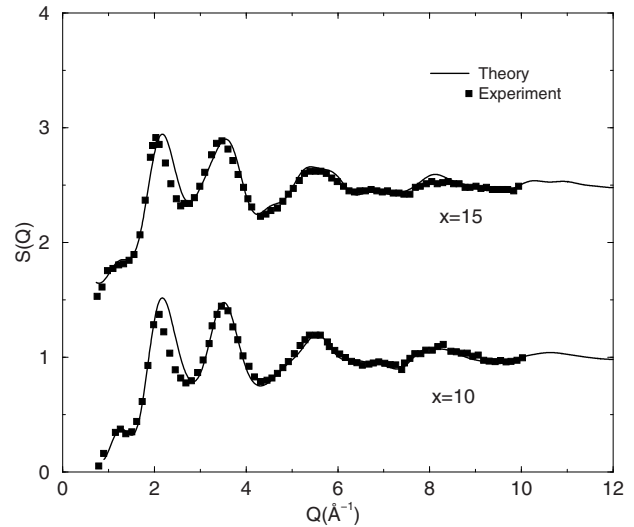


Fig. 7. Calculated total structure factor $S(Q)$ of $(\text{GeSe}_3)_{0.90}\text{Ag}_{0.10}$ and $(\text{GeSe}_3)_{0.85}\text{Ag}_{0.15}$ glasses compared to experimental [98] data. From [96].

Thus the introduction of Ag atoms induces shorter length-scale density fluctuations than the GeSe_3 glass. Moreover it disturbs the $\text{GeSe}_{4/2}$ network formation that leads to the fragmentation of $\text{GeSe}_{4/2}$ tetrahedra. From analysis of the partial structure factors it is apparent that the FSDP has contributions from all of the partials [96].

Where the Ag is concerned, to minimize the system energy, the Ag atoms sit preferentially near the midpoint of a line connecting (Ge or Se) atoms separated by about 5.0 Å, and we name these “Trapping Centers” or TC [97]. About 61% of Ag sites reside between a pair of Se, the rest involve one Ge. The distances between host pair atoms is between 4.7 to 5.2 Å and the bond length of the Ag to the atoms of the pair is in the range 2.4–2.6 Å. About 17% of Ag have a 2-fold Se neighboring pair, the rest of the Ag host pairs are under-coordinated. To verify the existence of these traps in an independent way, we introduced unbonded Ag at a variety of locations in a 64-atom amorphous Se model [99] at $T = 300$ K, so that the Ag could “probe” the energy landscape in an unbiased fashion and

without exception, the Ag became trapped between two Se host atoms with distances in the range we indicate above for the ternary glass.

7.3 Electronic features

A byproduct of any ab initio calculation are the Kohn-Sham [31] eigenvalues and eigenvectors, as in equation (4). Since structural and electronic properties are intimately related, an examination of electronic density of states provides additional insight about the properties of these materials. The electronic density of states (EDOS) of both models are calculated and analyzed by the inverse participation ratio (IPR), which provides a measure of spatial localization (the higher the IPR the more compactly localized the state). The EDOS are obtained by convolving each energy eigenvalue with suitably broadened Gaussian. In Figure 8 we report the calculated EDOS and the species projected density of states of $(\text{GeSe}_3)_{0.90}\text{Ag}_{0.10}$ and $(\text{GeSe}_3)_{0.85}\text{Ag}_{0.15}$ glasses. With the addition of Ag into $g\text{-GeSe}_3$, an intense peak, due to the Ag 4d electrons appears at about -3.47 eV as shown in Figure 8. The valence band exhibits three features. The two lowest bands between -14.8 eV and -7.0 eV originate from the atomic 4s-like states of Ge and Se partially hybridized to form bonding states to Ag atoms. The next band lying between -7.0 and 0.0 eV contains p like bonding states of Ge and Se and d like bonding states of Ag. The peak in the topmost valence region is due to the lone-pair 4p electrons of Se atoms. The Γ point optical gaps of $g\text{-}(\text{GeSe}_3)_{0.90}\text{Ag}_{0.10}$ and $g\text{-}(\text{GeSe}_3)_{0.85}\text{Ag}_{0.15}$ are respectively of the order of 1.20 and 1.26 eV. As the Ag content increases, the optical band gap slightly increases.

7.4 Dynamics of silver in $\text{GeSe}_3:\text{Ag}$ [97]

The dynamics of the Ag in the matrix is the special scientific interest of these materials. We used the code “Vienna Ab initio Software Package” “VASP” [37] for the MD simulations. Similar approximations have been used with success on GeSe_2 liquid and glass [46]. We carried such a calculation out earlier with the much faster code FIREBALL. We found that the two codes based on the same principles but differing vastly in detail gave very similar results both for the structure of the relaxed models and for dynamical simulation, always a reassuring sign for someone performing simulations. We use VASP to elucidate the nature of the TCs and associated silver dynamics [97].

Above $T = 300$ K, there is hopping between the TCs, but this is spatially non-uniform. We find that the TCs are non-uniformly distributed in space. Volumes with a high concentration of TCs have longer trap lifetimes than volumes with few or no TCs. The barriers between TCs that are close together tend to be small, enabling rapid hopping *within the high density region*, but the effect of a collection of TCs in close proximity is to create a strong barrier for the Ag to escape to another volume. Thus, one can introduce the notion of “supertraps” or cages built from

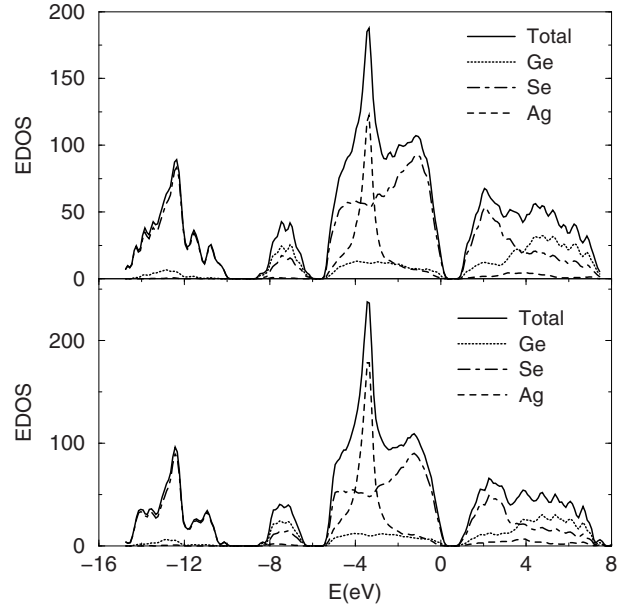


Fig. 8. Electronic density of states and species projected electronic density of states for Se, Ge, and Ag for $(\text{GeSe}_3)_{0.90}\text{Ag}_{0.10}$ (top panel) and $(\text{GeSe}_3)_{0.85}\text{Ag}_{0.15}$ (bottom panel) glasses. From [96].

more than one fundamental TC. The collective behavior of a set of TCs in close proximity is very different than the case of an isolated TC. The simulations reveal dynamics reminiscent of supercooled colloids [108] and diffusion of Li ions in silicate glass [109–111].

Silver dynamics was studied by constant-temperature Nosé-Hoover dynamics at 300 K and 700 K. Extended trajectories of 20 ps were obtained. At 300 K, silver is largely trapped: only 6 hopping events were observed. The silver traps fall into two categories. *Type 1* (32%) are strongly bound: 4 Ag atoms sit at single TC with no neighboring TC within a radius of 2.0 Å, and 7 Ag occupy two overlapping TCs with the host pairs making an angle of about 90° to each other. *Type 2* (68%) are oscillating between two or three closely spaced TCs. Figure 9 reveals the dynamics of the two types of Ag. In the top panel of Figure 9, dynamics of Ag_{213} (type 1) relative to the three TCs is shown. Initially it is trapped at TC(11-202) (between Ge_{11} and Se_{202}), the gradual decrease in the $\text{Ge}_{11}\text{-Se}_{202}$ distance pushes the Ag out and it is eventually trapped at two overlapping TCs [TC(60-202) and TC(11-98)]. Note the stabilization in the $\text{Se}_{60}\text{-Se}_{202}$ and $\text{Ge}_{11}\text{-Se}_{98}$ distances after Ag is trapped between the host atom-pair. The bottom panel of Figure 9 illustrates type 2 Ag motion. Ag_{228} is initially trapped at TC(107-142). It becomes unstable due to the motion of TC(142-150), (initially at 1.8 Å from Ag_{228}), and then a decrease in the $\text{Se}_{107}\text{-Se}_{142}$ distance moves it out of its initial TC. Eventually Ag_{228} is trapped between the two TCs [TC(142-150) and TC(32-129)] with an average distance of about 1.6 Å between them. The trajectory of Ag_{228} shows cage or “super-trapping” between two TCs. Note the larger fluctuations in the position of Ag as compared to type 1 Ag (trajectory of Ag_{213}). The hopping lengths between one TC to other TCs, in general

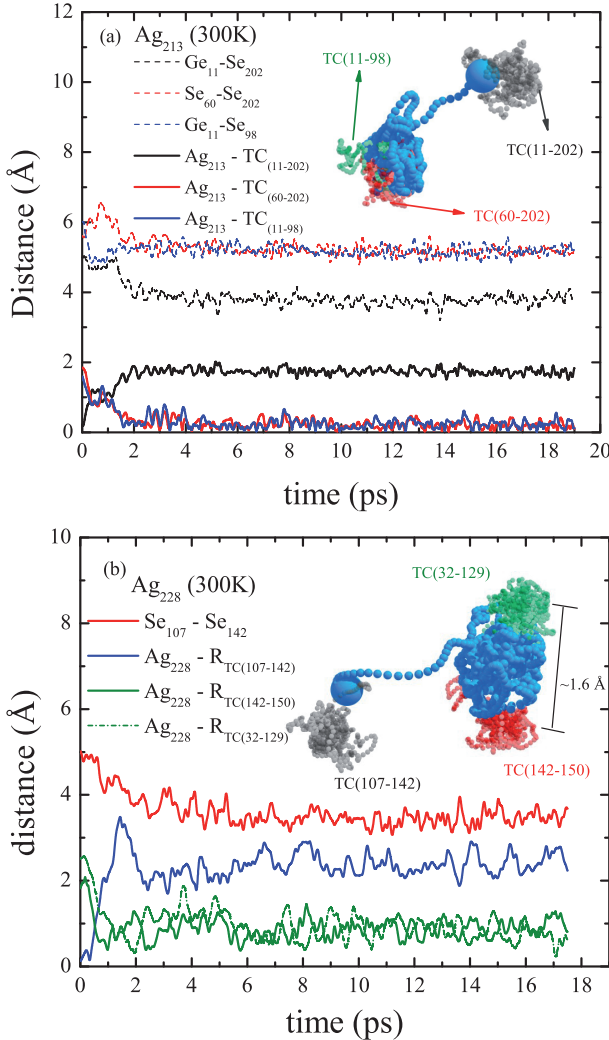


Fig. 9. Characteristic examples of silver dynamics: top: “Type 1” trap, bottom “Type 2” (see text). The inset shows the trajectories of Ag sites (blue) with the trajectories of neighboring TCs (grey, green and red). The motion is crudely oscillatory within a TC, and much more ballistic between traps. From [97].

depend upon the concentration of neighboring TCs. A larger number of neighboring TCs tends to confine the Ag in a smaller region (1.0 \AA) as in the two cases discussed above, while larger jumps are observed for Ag with lower concentration of neighboring TCs.

The mean-squared displacement of Ag at 700 K shows a linear increase with time, illustrating the diffusive nature of the Ag dynamics, consistent with the previous studies [96]. The Ag dynamics consists of a gradual drift away from the initial (fully relaxed) TC configurations, followed by hops between cages. There are 20 jumps observed, much larger than that for 300 K, as expected, with an average time period of *ca.* 7 ps between the hops. The hopping lengths vary between $1.5\text{--}4.0 \text{ \AA}$. We characterize such hopping dynamics in terms of the variation in the concentration of TCs n_{TC} around Ag sites. Figure 10 shows the displacement of Ag_{213} at 700 K. The hopping is apparent in the form of abrupt changes in the displace-

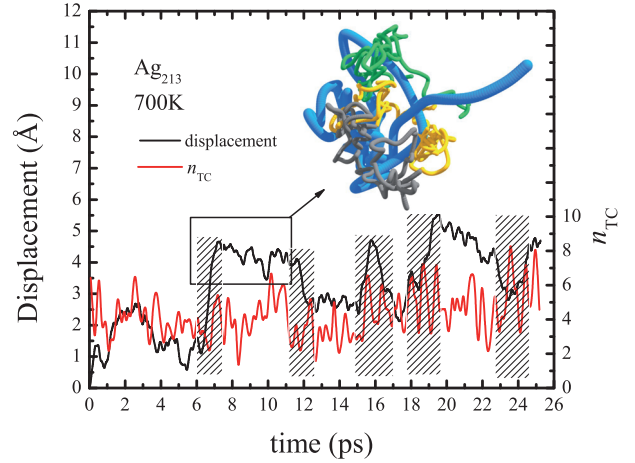


Fig. 10. Displacement of Ag_{213} from its initial starting position, and the average number n_{TC} of trapping centers surrounding Ag_{213} (within a radius of 4.0 \AA around the Ag atom). The shaded regions highlight the hops. The trajectory of Ag_{213} (blue) is shown along with those of three neighboring TCs (yellow, green and grey) in the time during which Ag is trapped after making a ‘jump’. Observe the creation and annihilation of TCs at 700 K. From [97].

ment. To understand these jumps, we counted the number of TCs surrounding the Ag site in a radius of 4.0 \AA . In Figure 10, the concentration of neighboring TCs is also plotted with the displacement. A correlation between the hops and the decrease in n_{TC} is apparent. The jumps tend to occur at times when either n_{TC} is low or exhibits a sudden decrease. Also, the figure reveals the significant impact of thermal fluctuations on the TCs and their density. The trajectory of Ag_{213} along with the trajectories of three neighboring TCs (inset) in the trapped region gives further insight into the nature of the trap. At higher temperature, the Ag sites are more unstable because of thermal fluctuations in the neighboring network and their higher thermal energies. It would require a higher density of TCs to confine the Ag dynamics. The hops can be considered as a spontaneous event, which may be triggered by a decrease in the concentration of neighboring TCs.

Figure 11 illustrates Ag motion at both temperatures. In equilibrium, the Ag at 300 K are confined on or in between the dense regions spanned by the TCs. Note that the volume fraction containing no TC is large at 300 K. At 700 K, TC are less concentrated owing to the thermal fluctuations in the host network, thus enhancing Ag diffusion. The Ag jumps between dense TCs regions (cages) is apparent. Such dynamics is quite similar to the hopping dynamics suggested for Li ions in silicate glasses [109,110], where the high mobility of Li ions is correlated with the decrease in the volume fraction of voids, which decreases the local atomic density around ion [108,111]. At 300 K, the TCs are relatively more stable and are distributed randomly as shown in Figure 11 in the form of dense and dilute regions, similar to the Scher-Lax-phillips traps [106]. One can view Figure 11 as a revealing a percolative process: at the higher temperature the trapping basins become

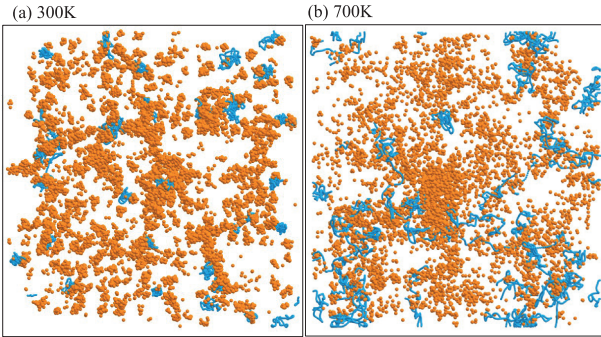


Fig. 11. Trajectories of TCs (orange) and all Ag (aqua) from MD simulation of about 6 ps length at (a) 300 K and (b) 700 K. Concentration of Ag sites around dense regions of TCs is apparent at 300 K and the Ag hops between the dense regions of TCs are clear at 700 K. Note the increase in the fraction of volume in the cell with TCs at 700 K relative to 300 K. From [97].

more extended and overlapping, until transport through the glass becomes possible.

8 Consequences of structural disorder on electrons

Thus far, we have discussed the “nuts and bolts” of how to form models, and we gave a few examples of specific materials. As an example of a different type of scientific question, we discuss the impact of structural disorder on the character of the electron states. We do this using current structural models (especially WWW models of a-Si), and the available electronic structure codes, including spectral techniques needed to handle large models.

8.1 Historical background

We begin with a tincture of historical context. Thanks to the celebrated work of Anderson, Mott and others, it became apparent in the late 1950’s that disorder could *localize* electrons. Here, localization means that electrons are confined to a finite volume of space. The relevant contrast is to crystals, for which Bloch’s theorem demonstrates that translational invariance *implies* extended states – for all the bands in the crystal. Anderson [115] initiated the mathematical study of localization due to disorder with the introduction of a tight-binding “Anderson model”:

$$H = \sum_{i=1}^n \varepsilon_i |i\rangle\langle i| + \sum_{i,j(nn)} V |i\rangle\langle j| \quad (11)$$

in which, ε_i are random diagonal energies selected from a uniform distribution of width W and hopping parameter V is a (site-independent) constant. The second sum usually is restricted to nearest-neighbors. This diagonal disorder is more akin to “alloy disorder” than topological disorder in an elemental system for which the ε_i are identical for all sites and the disorder modulates V alone. In equation (11) the ratio W/V characterizes the degree of disorder of the model. Owing to the tools available at the

time, the pioneers of the field carried out their work analytically. The calculations were mathematically difficult, and showed that for sufficient disorder in three dimensions, electronic states could be localized with sufficient disorder. The study of localization has been remarkably fruitful, and has proven to be important in the study of nonlinear dynamics [116], scattering of electromagnetic waves [117], the study of Bose-Einstein condensation [118], among others. The concept has even been invoked to explain the atmospheric phenomenon of Ball Lightning [119]. Thus, while the concept of localization was born in the context of disordered solids, it has taken on a life of its own and is now a mainstay of many scientific fields.

For the case of an amorphous semiconductor, such as a-Si, it was recognized early on that there is a localized-to-delocalized (LD) [2,115,120] transition near both the valence and conduction band tails in a-Si, since midgap defect states are known to be bound states (manifestly localized), and likewise, states well into the valence or conduction bands (beyond the mobility edges) are extended. While conceptually fundamental, this picture is qualitative, and offers limited assistance in interpreting experiments. The need for realistic calculations was made plain in Mott’s Nobel lecture [121], in which he states:

There is an extensive literature calculating the position of the mobility edge with various simple models, but it has not yet proved possible to do this for a continuous random network such as that postulated for SiO₂, As₂Se₃, amorphous Si or any amorphous material where the coordination number remains the same as in the crystal. This problem is going to be quite a challenge for the theoreticians – but up till now we depend on experiments for the answer, particularly those in which electrons are injected into a non-crystalline material and their drift mobilities measured [121].

8.2 Formulation

Such an undertaking requires (1) atomic level structural models of amorphous materials (eg., atomic coordinates) that faithfully reproduce experimental probes of structure, and (2) an ab initio or tight-binding prescription for computing the Hamiltonian H in some matrix representation, and finally means to at least partially diagonalize H in the chosen representation. Then we study the character of the eigenvectors of H for energies around the optical gap.

The WWW [5] models of a-Si appear to satisfy structural and vibrational experiments on the materials, and WWW models with as many as 10^5 atoms are now available. The WWW models use periodic boundary conditions, so that it is desirable to work with large models so that we can infer the properties of the localized states. Among the empirical Hamiltonians available for silicon, we adopt the tight-binding Hamiltonian of Kwon et al. [122]. Consistent with the spirit of the tight-binding approximation, this scheme allows for one s state and three p states per site. Here, we will report the spectral properties of a 4096 atom model of a-Si (which therefore has a tight-binding Hamiltonian matrix of dimension $D = 16\,384$).

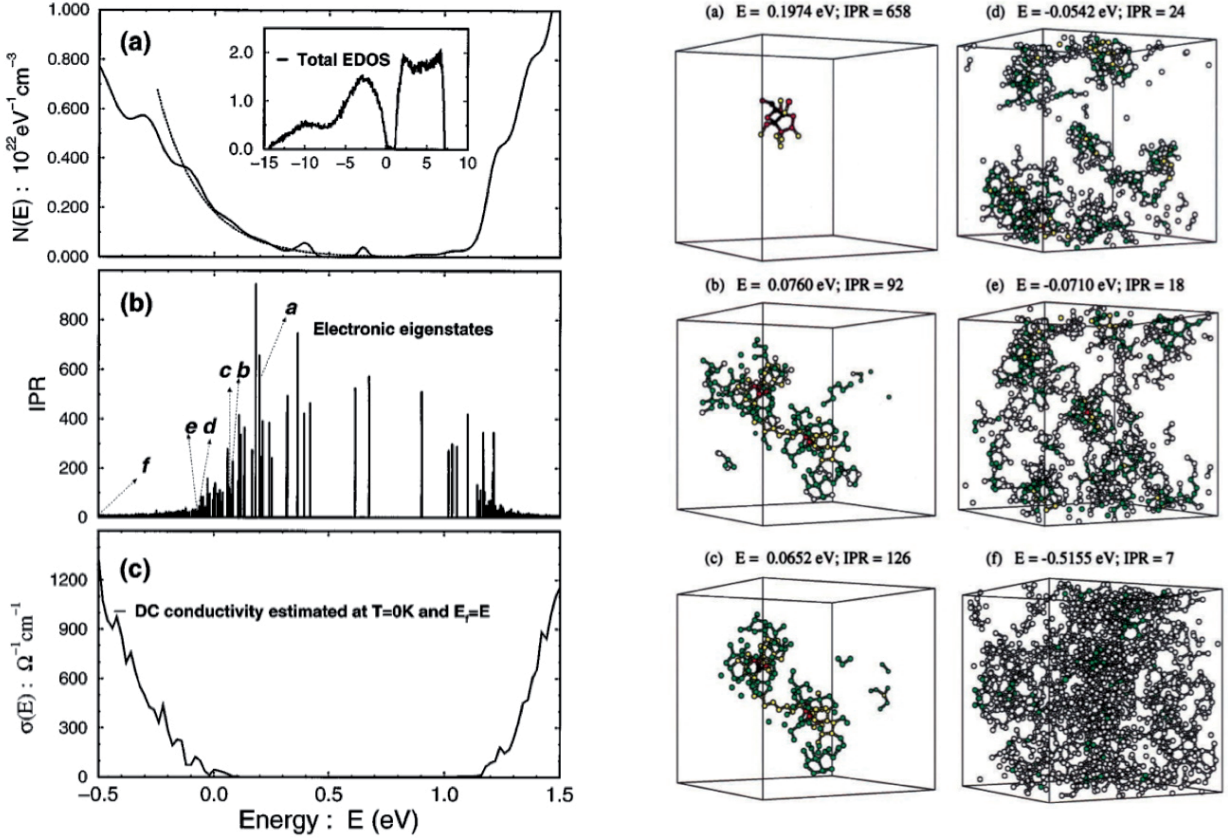


Fig. 12. Left: (a) electronic density of states of a-Si, (b) localization (from inverse participation ratio) and (c) conductivity from Kubo-Greenwood formula. Right: charge densities of the states indicated in (b) of left panel. Each atom shown is colored according to the fraction of total charge: black $>1/16$, red $>1/64$, yellow $>1/256$, green $>1/1024$, and white ($>1/1024$, such that at least 75% of the total charge is shown). The electronic states evolve from tightly localized (midgap) states (a) to filament-island localized (tail) states and finally to extended valence states (f). From [129].

With the H matrix in hand, we have to diagonalize it in some way. Numerical algorithms for “full diagonalization” (computing all eigenvalues and eigenvectors) are robust and mature. Modest computers can routinely compute all the eigenvalues and eigenvectors to machine precision (typically 10–15 digits) for matrices with dimension well into the thousands in minutes. At a practical level, these methods are so reliable that we recommend their use whenever possible. Their only limitation is that asymptotically (for large systems) CPU demand scales as D^3 and memory use scales as D^2 , at least. Approximate estimation of the global density of states is possible with recursion [123], maximum entropy [124] and kernel-polynomial [125] methods.

For our $D = 16384$ matrix, it is possible, but not easy, to use full diagonalization methods. It is also *unnecessary*, since we only care about a few hundred states near the Fermi level for this calculation. The power method, or the Lanczos [56,126] scheme, is an excellent choice for estimating eigenstates conjugate to extremal eigenvalues (meaning at the extreme low or high energy edges). However, for density-functional and tight-binding calculations, our interest does not lie with these extremal states, instead we require the eigenstates near the middle of the spectrum (around the optical gap). The trouble is that elementary

methods work very well for isolated states, but converge with impractical slowness for parts of the spectrum involving states nearly degenerate in energy (rather than giving a single state, one obtains a mixture in the nearly degenerate energy subspace). An effective approach is to work not with H , but instead with the energy-dependent operator [127] $\hat{G}(E) = (E - \hat{H})^{-1}$; this spreads the spectrum out effectively near energy E so that a simple Lanczos scheme becomes effective⁵. Other successful approaches exist [128].

In Figure 12, we illustrate the results of a calculation revealing many aspects of the Localized-Delocalized (LD) transition in a-Si [129]. The model used is a realistic 4096-atom WWW model due to Djordjevic, Thorpe and Wooten [130]. The model possesses a radial distribution function in agreement with experiment, and is entirely four-coordinated (thus, it exhibits no three-fold dangling bond defects). In the left panel of the figure, we plot the density of states, inverse participation ratio and a crude estimate of the electrical conductivity using the Kubo-Greenwood [131] formula. Highly localized defect states arising from large bond-angle distortions exist near

⁵ This approach, pioneered by engineers might have been discovered by physicists: G is the the electronic Green's function!

mid-gap, and valence and conduction band tails arise from the details of the structure of the model. The energies (and inverse participation ratios, which gauge the degree of localization), labeled by letters in the left panel are associated with the states that appear in the right panel.

To discuss the LD transition, let us begin with midgap state (a). Since it is localized, this state has a specific electronic energy and a restricted spatial extent. For energies incrementally closer to the mobility edge, two-island states appear: states (b) and (c), of Figure 12. Note also that the charge densities of states (b) and (c) are strikingly similar, though the states are orthogonal. Indeed, if one computes symmetric and anti-symmetric linear combinations of states (b) and (c), it is found that these approximately yield one island or the other. This hints that one can express the eigenstates near the gap as linear combinations of the islands. For energies closer yet to the mobility edge, the eigenstates may be decomposed into a large number of islands. Of course, the localization of the eigenstates decreases for an increasing number of islands until, eventually, the state becomes extended at the mobility edge.

These results lead to a qualitative and easily understood picture of the localized-to-extended transition. The island states arise from structural irregularities in the network sufficient to induce a localized island state with energy E and localization length ξ . If an island with energy E overlaps another spatially adjacent island with a similar energy, then perturbation theory implies that the system eigenstates near E are linear combinations of the island states with comparable energies. This also shows that eigenstates with similar energies tend to be spatially correlated, since an island with energy E may (by resonant mixing) contribute to other system eigenstates near E . The islands can be computed from the eigenstates, and have the interesting property that the island localization length ξ is only weakly dependent upon the energy. Thus, while there is a modest increase in ξ as one approaches the mobility edge, the decrease in localization in the eigenstates arises primarily from increasing numbers of islands, not from the islands becoming larger. At the mobility edge, the eigenstates consist qualitatively of islands extending through the entire cell, with large fluctuations in local charge density and as suggested by other work implying a multifractal character.

A byproduct of realistic (rather than model) calculations is that one can make detailed comparisons with experiments on the density of states, or quantities related to it. In a-Si, it has been shown that the existence of 1D filaments of connected short (long) bonds are associated with the valence (conduction) tail, and the existence of the filaments has been associated with the exponential (Urbach) form for the density of states known from experiments [132]. In a-Si, the correlation between structure (anomalous bond lengths) and band-tail electron states is pronounced as we show in Figure 13. Good quality models of a-Si are found to possess structural filaments, and their positions are strongly spatially correlated (short bonds tend to be connected to short bonds, and a similar statement for long bonds), as we illustrate in Figure 14 [133]. In

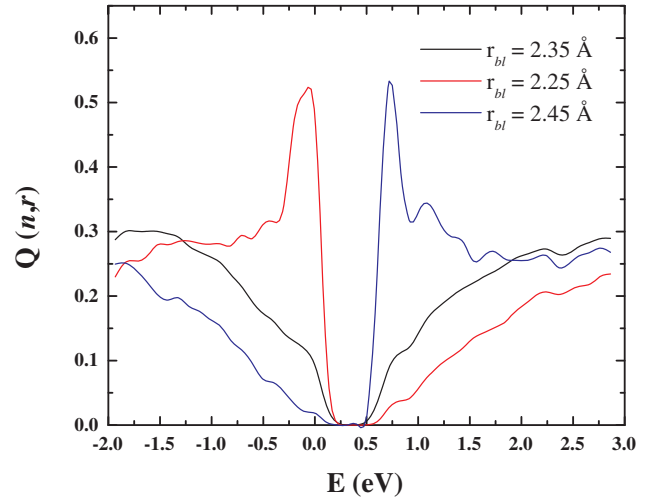


Fig. 13. Charge-weighted bond-lengths in a-Si, revealing that valence band-tail states arise from short bond-lengths, and conduction band-tail states from long bond-lengths. A 512-atom model was used with a density-functional Hamiltonian [132].

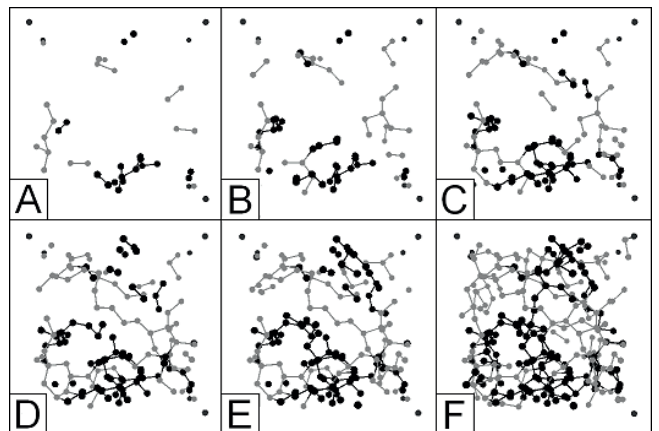


Fig. 14. Position of longest and shortest bonds in 512-atom WWW model [130]. (A) 1%, (B) 2%, (C) 3%, (D) 4%, (E) 5% and (F) 8% shortest (dark) and longest (light) bonds. Note that short and long bonds are strongly spatially correlated (there is, for example, obvious filamentary connectivity in D). From [133].

the language of the Anderson model [115], this would be an example of correlated disorder. Aoki [135] predicted a filamentary character and fractal self-similarity at the mobility edge in Anderson models. In realistic calculations for a-Si at least, the filamentary character of states seems to persist for energies well beyond the mobility edge into the gap, and in fact is strongest near the middle of the gap.

8.3 Universality

In this section we briefly consider some generic spectral manifestations of disorder, beyond electrons [136]. By directly computing the eigenstates for energies around spectral gaps for electrons in a topologically disordered network, Anderson models, classical lattice vibrations for

models with mass and topological disorder, it has been shown that the qualitative nature of the localized-to-extended transition is universal in the sense that all these systems have important features in common: the most localized states are single island states, and for energies approaching the mobility edge, the number of constituent islands increases until they inhomogeneously fill space at the mobility edge. This work justifies the many studies of Anderson models, which indeed capture many qualitative features of localization and the localized-to-extended transition. Detailed, system-specific properties (such as the nature of defect and tail states) require accurate calculation on large, realistic structural models.

The universal picture of the internal structure of localized eigenstates leads to the conclusion that different localized states tend to be correlated with each other (especially for those with near-adjacent eigenvalues) as a result of the same islands of charge density (or vibrational amplitude) appearing in different eigenstates. Correlations between localized states (particularly near the mobility edge) had been anticipated, but this work is the first to demonstrate unambiguously the structural origin of such correlations and its occurrence for diverse realistic models. The existence of such (strong) correlations has a number of consequences for the physical behaviour associated with localized eigenstates.

The LD transition appears in diverse contexts in disordered systems. To see how general is the picture of localized eigenstates comprised of bare island states that was found in the study of electron states in a-Si, we have also considered a simple-cubic-lattice Anderson electron model, atomic vibrations in a force-constant-disordered FCC lattice model and in a realistic, topologically disordered model of a-Si and, to explore the role of long-range (Coulombic) interactions, in a 1650-atom realistic model of a-SiO₂. In Figure 15a, we show three superposed critical eigenstates, adjacent in energy, for the Anderson electron model. This figure illustrates that even critical eigenvectors are still clearly composed of islands. Three adjacent-energy localized vibrational eigenvectors showing island structures are shown for the model of a-SiO₂ in Figure 15b, of a force-constant-disordered FCC lattice in Figure 15c and for the model of a-Si in Figure 15d. It is evident, therefore, that systems with highly distinct types of disorder possess qualitatively similar island-like internal structures of localized eigenstates. For all the model systems discussed in this paper, states in the gap, far from the band edge, are highly localized single-island states, while for energies in a band tail multi-island localized states appear; these eigenvectors may be decomposed into primitive islands, which may appear at the same position in several different adjacent-energy eigenvectors. The islands become more numerous, but only slightly spatially larger as the energy approaches the critical LD energy. Moreover, these conclusions appear to hold for either long-range or short-range interactions, for electronic and vibrational eigenstates, and for diverse manifestations of disorder in both realistic and toy models.

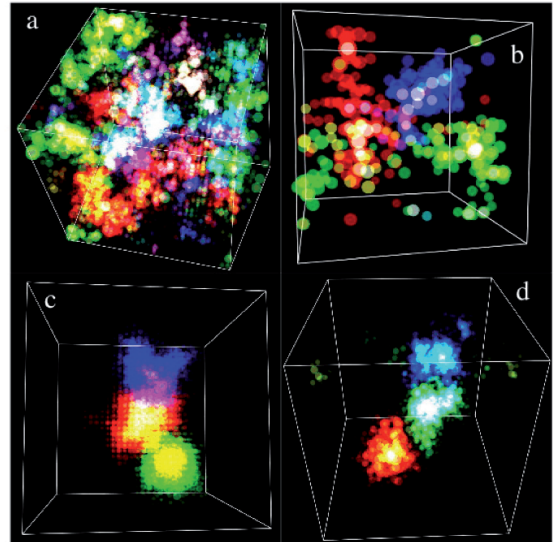


Fig. 15. Universality of localized-eigenstate structure for sets of three localized eigenstates (red, green and blue) for various systems, showing spatial overlap of islands. Regions where two islands overlap are shown with secondary colors and overlap between three islands is shown in white: (a) three adjacent-energy eigenvectors taken from the band centre for the electronic Anderson model on a simple cubic lattice with the critical ratio of the range of on-site disorder of width W to the off-diagonal interaction, V , i.e. $W/V = 16.5$, sufficient to localize all states in the band. These are critical eigenvectors of the model, and are clearly constructed from islands. The appearance of the same islands in consecutive eigenstates is clearly evident. (b) Three adjacent-energy vibrational eigenvectors of a 1650-atom vitreous silica model. Three regions, that are mainly red, green and blue, can be seen, and each of these has a white centre, indicating overlap of the three eigenvectors at these points. (c) Three adjacent-energy vibrational eigenvectors on a 48-site FCC lattice with force constants taken from a uniform distribution of width 2.0 and average value 1.0 (the crystal has a force-constant value of unity). The overlapping island states are less isotropic because of the underlying lattice. (d) Three adjacent-energy vibrational eigenvectors (red, green, blue) of a 10^4 -atom model of a-Si, again showing strongly overlapping islands. From reference [136].

8.4 Wannier functions and density matrix for disordered systems

Wannier [137] introduced a real-space localized representation of electrons, now called the Wannier representation in 1937. Until recently, the orbitals enabling this, the Wannier functions, were mostly used in formal developments, and in transport theory. With the introduction of Kohl's Principle of Nearsightedness [6], the electronic locality of the insulating state has become recognized as a fundamental feature of matter, and the Wannier representation has taken on a new significance. Prodan and Kohn [138] have shown that the local electronic properties arise from the potential only at nearby points, clarify why Pauling's concept of the chemical bond [139] is so useful, and offer the mathematical link between band and

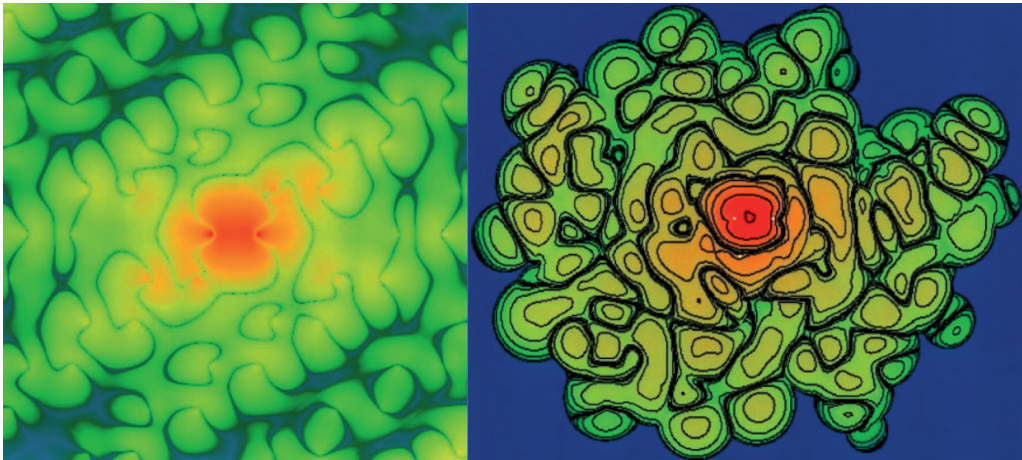


Fig. 16. Orthonormal Wannier functions: left panel, from a 512-atom model of diamond within the (110) plane; right panel: one function from a 4096 atom model of amorphous silicon. In both panels, maximum charge is indicated by red, minimum by blue. Note the bond charge near the center of both images. The dark blue or black lines are nodal lines. The complex nodal structure is required to enforce orthogonality between distinct functions. From references [142,144].

bond pictures. The mathematical tools required to quantify these notions are the Wannier functions and the density matrix. In the last fifteen years, there has been a separate resurgence of interest in Wannier functions [140] as an efficient tool for computing materials properties, including amorphous materials. Boys molecular orbitals [141] in quantum chemistry are conceptually similar to the Wannier functions.

Wannier functions are a unitary transformation of the Bloch states in crystals. For a given crystal, the Wannier functions are not unique: different unitary transformations yield Wannier functions with different spatial decay properties. A breakthrough for the practical use of Wannier functions was the creation of a method to compute the most-localized Wannier functions [140]. These functions are exponentially localized in space for insulators. The utility of the Wannier functions arises from their decay: in the Wannier representation, matrix elements between well-separated parts of an insulator vanish. The same is not true of Bloch states! This is useful for computations requiring large models, such as amorphous insulators or biomolecules: because the band energy can be written as a trace: $E_{band} = \text{Tr}(\rho H)$, the range of the energy (and forces) are determined by the range of the density matrix (or Wannier functions): only that subset of Wannier functions overlapping a given site are required to compute the local energy or the force at that site. For amorphous materials, it has also been argued that the network defined by the centers of Wannier functions is a preferred way to define coordination – better than simple, but arbitrary, geometrical criteria [143]. Technically, since there are no Bloch states, by definition, in an amorphous material, these are called generalized Wannier functions.

Wannier functions have recently been obtained in amorphous diamond, and a-Si, by direct construction from the electronic eigenstates [143], and also using order-N projection methods [144]. It has been demonstrated that Wannier functions in a-Si decay exponentially, and with a rate close to that of crystalline Si (diamond). In Fig-

ure 16, we show a 2D slice of selected Wannier functions computed for amorphous Si and diamond. These states are orthonormal: $\int d^3x w_n^*(\mathbf{x})w_m(\mathbf{x}) = \delta_{mn}$, where w_n is the n th Wannier function, and the integral extends over all space, with δ_{nm} being Kronecker's symbol. Elements of both the chemical bond and band picture can be observed. First, there is clearly bond charge displayed, and this is quite concentrated between two atoms. However, there is also complex diffuse charge in the state extending out over several neighbor distances. In the case of the crystal, it is found that the decay rate is weakly anisotropic (a slower decay along the bond than orthogonal to it). One could say that the utility of the bond picture arises from the large accumulation of bond charge, whereas the solid state nature is associated with the long-range decay. Note the interesting symmetries in the crystal absent in the amorphous case. For Wannier functions centered on highly irregular sites (with especially anomalous bonding), the behavior of the function is distinctive near the defect [142], yet the asymptotic decay of all functions far from the center is similar to typical functions, and exponential in character.

A representation-independent gauge of the locality of quantum mechanics in any material is the decay of the off-diagonal elements of the density matrix in position representation [146]:

$$\rho(\mathbf{x}, \mathbf{x}') = \langle \mathbf{x} | \hat{\rho} | \mathbf{x}' \rangle, \quad (12)$$

where $\hat{\rho}$ is the single-particle density operator, which can be written equally well in an energy or Wannier representation:

$$\rho(\mathbf{x}, \mathbf{x}') = 2 \sum_{n-occ} \psi_n^*(\mathbf{x}) \psi_n(\mathbf{x}') = 2 \sum_n w_n^*(\mathbf{x}) w_n(\mathbf{x}'). \quad (13)$$

It has long been believed for systems with a gap that [145]:

$$\rho(\mathbf{x}, \mathbf{x}') \sim \exp(-\gamma |\mathbf{x} - \mathbf{x}'|) \quad (14)$$

for large $|\mathbf{x} - \mathbf{x}'|$.

The reason for this decay is destructive wave-mechanical interference [6]. By direct calculation of equation (13), it has been shown that the density matrix for crystalline Si and a-Si decay with similar decay rates $\gamma \approx 0.49 \text{ \AA}^{-1}$ for crystal and $\gamma \approx 0.45 \text{ \AA}^{-1}$ for a-Si). Long ago, Kohn [145] made a crude estimate for the decay of the density matrix in insulators, estimating the rate γ (in Eq. (14)) as:

$$\gamma = (2E_g m / \hbar^2)^{1/2} \quad (15)$$

with E_g being the optical gap, and m the electron mass, in surprisingly plausible agreement with detailed calculations [146]⁶. It is surprising at first glance that amorphous Si and crystalline Si should have such similar decays: one might naively expect considerably more scattering and interference for the disordered network (and thus expect a larger γ), but this is not so [144,146]. The calculation was repeated for diamond and amorphous diamond, with analogous results. Decay rates γ are fundamental constants of these materials, gauging the locality of the materials electronic structure, and suggesting that clusters of at least 5–6 Å in size should capture the gross effects of the electronic structure, and an accuracy of order 1% would be expected for local properties at the center of a cluster with radius $\gtrsim 10 \text{ \AA}$. The Wannier functions of Figure 16 decay at a rate similar to the density matrix. Naturally, the volumes required for electronic calculations depend upon the material, and can apparently be roughly approximated by Kohn's expression equation (15). These calculations offer rigorous justification for local approaches in amorphous semiconductors, the rationale for which was not obvious even to Ziman [149]. The decay of these functions is also of significance for computation, since efficient order- N methods exploit real-space localized representations with either the density matrix or Wannier functions.

9 Conclusion

The purpose of this paper has been to illustrate several aspects of the theory of disordered materials. In my view, the field is a happy convergence of scientifically interesting problems, often with distinct technological potential. This area utilizes many of the tools of theoretical and computational science. This is a field in which modeling and theoretical analysis are particularly helpful, as experiments alone are usually not able to unambiguously determine even the structure of amorphous materials.

I hope that it is clear that there is room for development in practically every aspect of the field touched upon in this paper. The pressing need for improving amorphous materials for practical application is a driving force that will keep researchers active in this field for the foreseeable future.

⁶ Two more recent calculations giving more detailed functional forms are references [147] and [148].

This paper requires more words of acknowledgement than usual. First, most of what I present is work that I have published with former and current post docs, students and colleagues. These include P. Biswas, X. Zhang, J. Dong, D.N. Tafen, J. Ludlam, F. Inam, I. Chaudhuri, M. Zhang, M. Cobb, U. Stephan, N. Mousseau, R.L. Cappelletti, R.M. Martin, M. Mitkova, S.N. Taraskin, S.R. Elliott, J.R. Abelson and P.M. Voyles. I also want to specifically thank Michael Kozicki for his support and collaboration on the Programmable Metalization Cell and for the use of Figure 6. I have benefited tremendously from support from the National Science Foundation under grants DMR-0600073 and DMR-0605890 (and predecessor NSF awards), and the US Army Research Office and US Army Research Laboratory under Cooperative Agreement Number W911NF-0-2-0026. I thank Axon Technologies Corp. for support during early work on the silver chalcogenide glasses. I thank the Leverhulme Trust (UK) and the NSF International Materials Institute for New Functionalities in Glass under award DMR-0409588 for supporting aspects of this work carried out in Cambridge. I thank Trinity College, Cambridge, for hospitality.

References

1. S.R. Elliott, *Physics of Disordered Materials*, 2nd edn. (Longman, Essex, UK, 1990)
2. R. Zallen, *Physics of Amorphous Solids* (Wiley, New York, 1983)
3. R. Waser, M. Aono, *Nature Materials* **6**, 833 (2007); M. Mitkova, M.N. Kozicki, *J. Non. Cryst. Sol.* **299–302**, 1023 (2002)
4. M. Wuttig, N. Yamada, *Nature Materials* **6**, 824 (2007)
5. F. Wooten, D. Weaire, in *Modeling tetrahedrally bonded random networks by computer*, Solid State Physics, edited by H. Ehrenreich, D. Turnbull, F. Seitz (New York: Academic, 1987), p. 40; F. Wooten, K. Winer, D. Weaire, *Phys. Rev. Lett.* **54**, 1392 (1985)
6. W. Kohn, *Rev. Mod. Phys.* **71**, 1253 (1999)
7. F. Stillinger, *Phys. Rev. E* **59**, 48 (1999)
8. V. Ramakrishnan, *Nature* **407**, 21 (2000)
9. M.M.J. Treacy, J.M. Gibson, L. Fan, D.J. Paterson, I. McNulty, *Rep. Prog. Phys.* **68**, 2899 (2005)
10. A.E. Carlsson, in *Solid State Physics, Adv. in research and Applications*, edited by H. Ehrenreich, D. Turnbull (Academic, New York, 1990), Vol. 43, p. 1
11. D.A. Drabold, P.A. Fedders, P. Stumm, *Phys. Rev. Lett.* **72**, 2666 (1994)
12. P.N. Keating, *Phys. Rev.* **145**, 637 (1966)
13. A. Trave, P. Tangney, S. Scandolo, A. Pasquarello, R. Car, *Phys. Rev. Lett.* **89**, 245504 (2002)
14. B.W.H. Vanbeest, G.J. Kramer, R.A. Vansanten, *Phys. Rev. Lett.* **64**, 1955 (1990)
15. For example, K. Vollmayr, W. Kob, K. Binder, *Phys. Rev. B* **54**, 15808 (1996); see also K. Binder, W. Kob, *Glassy materials and disordered solids: An introduction to their statistical mechanics* (World Scientific, Singapore, 2005)
16. W.A. Harrison, *Electronic Structure and the Properties of Solids: The Physics of the Chemical Bond* (Freeman, San Francisco, 1980)
17. W.M. Foulkes, R. Haydock, *Phys. Rev. B* **39**, 12520 (1989)
18. O.F. Sankey, R.E. Allen, *Phys. Rev. B* **33**, 7164 (1985)

19. L. Goodwin et al., *Europhys. Lett.* **9**, 701 (1989), see also J. Mercer, M.Y. Chou, *Phys. Rev. B* **47**, 9366 (1993)
20. C.H. Xu et al., *J. Phys. Cond. Matt.* **4**, 6047 (1992)
21. G. Seifert, R. Jones, *Z. Phys. D* **20**, 77 (1991); M. Elstner, T. Frauenheim, E. Kaxiras, G. Seifert, S. Suhai, *Phys. Stat. Sol. (b)* **217**, 357 (2000)
22. P. Ordejón, *Comput. Mater. Sci.* **12**, 157 (1998); S. Goedecker, *Rev. Mod. Phys.* **71**, 1085 (1999)
23. L. Colombo, *Rivista Del Nuovo Cimento* **28**, 1 (2005)
24. L.J. Lewis, N. Mousseau, *Comp. Matl. Science* **12**, 210 (1998)
25. L. Colombo, M. Rosati, *Comput. Phys. Comm.* **128**, 108 (2000)
26. D.R. Hartree, *Proc. Cambridge Phil. Soc.* **24**, 89 (1928)
27. F. Fock, *Z. Phys.* **61**, 126 (1930)
28. M. Born, J.R. Oppenheimer, *Ann. Phys.* **84**, 457 (1927)
29. J. Kohanoff, *Electronic structure calculations for solids and molecules* (Cambridge University Press, Cambridge, 2006)
30. E. Fermi, *Z. Phys.* **48**, 73 (1927); L.H. Thomas, *Proc. Cambridge Phil. Soc.* **23**, 542 (1927)
31. P. Hohenberg, W. Kohn, *Phys. Rev.* **136**, B864 (1964); W. Kohn, L.J. Sham, *Phys. Rev.* **140**, A1133 (1965)
32. R.M. Martin, *Electronic Structure: Basic Theory and Practical Methods* (Cambridge University Press, Cambridge, 2004)
33. D.M. Ceperley, B.J. Alder, *Phys. Rev. Lett.* **45**, 566 (1980)
34. See M.S. Hybertsen, S.G. Louie, *Phys. Rev. B* **34**, 5390 (1986)
35. E. Artacho et al., *J. Phys.: Condens. Matter* **20**, 064208 (2008); J.M. Soler, E. Artacho, J.D. Gale, A. Garca, J. Junquera, P. Ordejón, D. Sanchez-Portal, *J. Phys.: Condens. Matter* **14**, 2745 (2002); <http://www.uam.es/departamentos/ciencias/fismateriac/siesta/>
36. O.F. Sankey, D.J. Niklewski, *Phys. Rev. B* **40**, 3979 (1989); J.P. Lewis, K.R. Glaesman, G.A. Voth, J. Fritsch, A.A. Demkov, J. Ortega, O.F. Sankey, *Phys. Rev. B* **64**, 195103 (2001); <http://www.fireball-dft.org/web/fireballHome>
37. G. Kresse, J. Furthmüller, *Phys. Rev. B* **54**, 11169 (1996); <http://cms.mpi.univie.ac.at/vasp/>
38. M.C. Payne, M.P. Teter, D.C. Allan, T.A. Arias, J.D. Joannopoulos, *Rev. Mod. Phys.* **64**, 1045 (1992); www.castep.org
39. R. Car, M. Parrinello, *Phys. Rev. Lett.* **55**, 2471 (1985); www.cpmd.org
40. <http://www.quantum-espresso.org/>
41. <http://www.abinit.org/>
42. E. Holmberg, *Astrophys. J.* **94**, 385 (1941)
43. I thank Prof. Tom Statler for pointing this out
44. M.P. Allen, D.J. Tildesley, *Computer simulation of liquids* (Oxford University Press, Oxford, 1987)
45. J. Sarnthein, A. Pasquarello, R. Car, *Phys. Rev. Lett.* **74**, 4682 (1995)
46. C. Massobrio, A. Pasquarello, *Phys. Rev. B* **64**, 144205 (2001); L. Giacomazzi, C. Massobrio, A. Pasquarello, *Phys. Rev. B* **75**, 174207/1-13 (2007)
47. M. Cobb, D.A. Drabold, R.L. Cappelletti, *Phys. Rev. B* **54**, 12162 (1996)
48. G. Fabricius et al., *Phys. Rev. B* **60**, 16283 (1999)
49. N. Jakse, A. Pasturei, *Phys. Rev. Lett.* **99**, 205702 (2007)
50. G.T. Barkema, N. Mousseau, *Phys. Rev. Lett.* **77**, 4358 (1996)
51. N. Mousseau, G.T. Barkema, *Phys. Rev. E* **57**, 2419 (1998)
52. N. Mousseau, L.J. Lewis, *Phys. Rev. Lett.* **78**, 1484 (1997)
53. N. Mousseau, L.J. Lewis, *Phys. Rev. B* **56**, 9461 (1997)
54. J.P.K. Doye, D.J. Wales, *Z. Phys. D* **40**, 194 (1997)
55. R. Malek, N. Mousseau, *Phys. Rev. E* **62**, 7723 (2000)
56. C. Lanczos, *Applied Analysis* (Prentice Hall, New York, 1956)
57. R. Kaplow, T.A. Rowe, B.L. Averbach, *Phys. Rev.* **168**, 1068 (1968)
58. R.L. McGreevy, L. Pusztai, *Mol. Sim.* **1**, 359 (1988)
59. A.K. Soper, *Phys. Rev. B* **72**, 104204 (2005)
60. G. Evrard, L. Pusztai, *J. Phys. Cond. Matt.* **17**, S1 (2005)
61. N. Metropolis, A.W. Rosenbluth, M.N. Rosenbluth, A.H. Teller, E. Teller, *J. Chem. Phys.* **21**, 1087 (1953)
62. G. Opletal et al., *J. Phys.: Condens. Matter* **17**, 2605 (2005)
63. A. Jack, M. Levitt, *M. Acta Crystallogr. A* **34**, 931 (1978)
64. P. Biswas, D.N. Tafen, F. Inam, B. Cai, D.A. Drabold, *J. Phys. Cond. Matt.* **21**, 084207 (2009)
65. P. Biswas, D.N. Tafen, R. Atta-Fynn, D.A. Drabold, *J. Phys. Cond. Matter* **16**, S5173 (2004); P. Biswas, D. N. Tafen, D.A. Drabold, *Phys. Rev. B* **71**, 054204 (2005)
66. R.L. Cappelletti, M. Cobb, D.A. Drabold, W.A. Kamitakahara, *Phys. Rev. B* **52**, 9133 (1995)
67. P. Biswas, R. Atta-Fynn, D.A. Drabold, *Phys. Rev. B* **76**, 125210 (2007)
68. E.T. Jaynes, *Probability Theory: The Logic of Science* (Cambridge University Press, Cambridge, 2003)
69. G.L. Bretthorst, *Bayesian Spectrum Analysis and Parameter Estimation* (Springer, New York, 1988). Available at <http://www.bayes.wustl.edu>
70. M. Habeck, W. Rieping, M. Nilges, *Proc. Nat. Acad. Sci. USA* **103**, 1756 (2006)
71. N. Mousseau, G.T. Barkema, *J. Phys. Cond. Matt.* **16**, S5183 (2004)
72. N. Mousseau, G.T. Barkema, *Phys. Rev. B* **61**, 1898 (2000)
73. S. Nakhmanson, P. Voyles, N. Mousseau, G. Barkema, D.A. Drabold, *Phys. Rev. B* **63**, 235207 (2001)
74. M.F. Thorpe, S.W. de Leeuw, *Phys. Rev. B* **33**, 8490 (1986)
75. P.M. Voyles, N. Zotov, S.M. Nakhmanson, D.A. Drabold, J.M. Gibson, M.M.J. Treacy, P. Kebinski, *J. Appl. Phys.* **90**, 4437 (2001)
76. D.N. Tafen, D.A. Drabold, *Phys. Rev. B* **68**, 165208 (2003); D.N. Tafen, D.A. Drabold, *Phys. Rev. B* **71**, 054206 (2005)
77. R.L.C. Vink, G.T. Barkema, *Phys. Rev. B* **67**, 245201 (2003)
78. M.G. Tucker, D.A. Keen, M.T. Dove, K. Trachenko, *J. Phys. Cond. Matt.* **17**, S67 (2005); R.L. Mozz, B.E. Warren, *J. Appl. Crystallogr.* **2**, 164 (1969); R. Pettifer et al., *J. Non.-Cryst. Sol.* **106**, 408 (1988); R.F. Pettifer, R. Dupree, I. Farnan, U. Sternberg, *J. Non-Cryst. Solids* **106**, 408 (1988)
79. P.A.V. Johnson, A.C. Wright, R.N. Sinclair, *J. Non-Cryst. Sol.* **58**, 109 (1983)
80. X. Zhang, Ph.D. thesis, Ohio University, 2001
81. N. de la Rosa et al., *Phys. Rev. B* **33**, 4094 (1986)

82. I. Santos, W. Windl, L. Pelaz, L.A. Marques, D.A. Drabold, submitted to Phys. Rev. Lett.
83. P. Krecmer, A.M. Moulin, R.J. Stephenson, T. Rayment, M.E. Welland, S.R. Elliott, Science **277**, 1799 (1997)
84. G. Ceder, M. Doyle, P. Arota, Y. Fuentes, MRS Bulletin **27**, 619 (2002)
85. T. Kawaguchi, S. Maruno, S.R. Elliott, J. Appl. Phys. **79**, 9096 (1996)
86. M. Kawasaki, J. Kawamura, Y. Nakamura, M. Aniya, Solid State Ionics **123**, 259 (1999)
87. H. Iyetomi, P. Vashishta, R.K. Kalia, J. Non. Cryst. Sol. **262**, 135 (2000)
88. S.C. Moss, D.L. Price, *Physics of disordered materials*, edited by D. Adler, H. Fritzsche, S.R. Ovshinsky (Plenum, New York, 1985), p. 77
89. J. Habasaki, K.L. Ngai, Y. Hiwatari, J. Chem. Phys. **122**, 054507 (2005)
90. T. Kawaguchi, Photo-induced deposition of silver particles on amorphous semiconductors, in *Photo-induced metastability in amorphous semiconductors*, edited by A.V. Kolobov (Wiley, Weinheim, 2003), p. 182
91. M. Mitkova, Real time optical recording on thin films of amorphous semiconductors, in *Insulating and semiconducting glasses*, edited by P. Boolchand (World Scientific, Singapore, 2000), p. 813
92. Y. Wang, M. Mitkova, D.G. Georgiev, S. Mamedov, P. Boolchand, J. Phys. Cond. Matt. **15**, S1573 (2003)
93. M.N. Kozicki, M. Park, M. Mitkova, IEEE Trans. Nanotech. **4**, 331 (2005)
94. J.S. Romero, A.G. Fitzgeralds, M.J. Rose, Appl. Surf. Sci. **234**, 369 (2004)
95. K. Terabe, T. Hasegawa, T. Nakayama, M.A. Aono, Nature **433**, 47 (2005)
96. D.N. Tafen, D.A. Drabold, M. Mitkova, Phys. Status Solidi B **242**, R55 (2005); De Nyago Tafen, D.A. Drabold, M. Mitkova, Phys. Rev. B **72**, 054206 (2005)
97. I. Chaudhuri, F. Inam, D.A. Drabold, Phys. Rev. B (in press), www.arxiv.org/abs/0811.1982
98. A. Piarristeguy, M. Fontana, B. Arcondo, J. Non. Cryst. Sol. **332**, 1 (2003)
99. X. Zhang, D. Drabold, Intl. J. Modern Phys. B, **15**, 3190 (2001); X. Zhang, D.A. Drabold, Phys. Rev. Lett. **83**, 5042 (1999)
100. M.N. Kozicki, M. Mitkova, J. Non-Cryst. Solids **352**, 567 (2006)
101. M. Kawasaki, J. Kawamura, Y. Nakamura, M. Aniya, Solid State Ionics **123**, 259 (1999)
102. A.V. Kolobov, S.R. Elliott, Advances in Physics **40**, 625 (1991)
103. E. Bychkov, V. Tsegelnik, Y. Vlasov, A. Pradel, M. Ribes, J. Non-Cryst. Solids **208**, 1 (1996)
104. M.A. Urena, A.A. Piarristeguy, M. Fontana, B. Arcondo, Solid State Ionics **176**, 505 (2005)
105. S.R. Elliott, J. Non-Cryst. Solids **172–174**, 1343 (1994)
106. J.C. Phillips, Rep. Prog. Phys. **59**, 1133 (1996)
107. S. Adams, J. Swenson, Phys. Rev. Lett. **84**, 4144 (2000)
108. E.R. Weeks, D.A. Weitz, Phys. Rev. Lett. **89**, 0957704 (2002)
109. J. Habasaki, I. Okada, Y. Hiwatari, Phys. Rev. B **55**, 6309 (1997)
110. J. Habasaki, Y. Hiwatari, Phys. Rev. E **59**, 6962 (1999)
111. J. Habasaki, K.L. Ngai, Y. Hiwatari, Phys. Rev. E **66**, 021205 (2002)
112. C. Massobrio, A. Pasquarello, Phys. Rev. B **64**, 144205 (2001)
113. L. Giacomazzi, C. Massobrio, A. Pasquarello, Phys. Rev. B **75**, 1 (2007)
114. D.A. Drabold, T.A. Abtew, F. Inam, Y. Pan, J. Non-Cryst. Solids **354**, 2149 (2008)
115. P.W. Anderson, Phys. Rev. **109**, 1492 (1958)
116. S. Graffi, M. Lenci, J. Stat. Phys. **116**, 821 (2004)
117. D.S. Wiersma et al., Nature **390**, 671 (1997)
118. G. Roati et al., Nature **453**, 895 (2008)
119. K. Tanaka, M. Tanaka, Appl. Phys. Lett. **71**, 3793 (1997)
120. N.F. Mott, *Electronic Processes in Noncrystalline Materials* (Oxford University Press, Oxford, 1978)
121. N.F. Mott, Rev. Mod. Phys. **50**, 203 (1978); http://nobelprize.org/nobel_prizes/physics/laureates/1977/mott-lecture.html
122. I. Kwon et al., Phys. Rev. B **49**, 7242 (1994)
123. R. Haydock, Solid State Phys. **35**, 215 (1980)
124. D.A. Drabold, O.F. Sankey, Phys. Rev. Lett. **70**, 3631 (1993)
125. R.N. Silver et al., J. Comp. Phys. **124**, 115 (1996); A. Weiße, G. Wellein, A. Alvermann, H. Fehske, Rev. Mod. Phys. **78**, 275 (2006)
126. O.F. Sankey, D.A. Drabold, A. Gibson, Phys. Rev. B **50**, 1376 (1994)
127. M.T. Jones, M.L. Patrick, SIAM J. Matrix Anal. Appl. **14**, 553 (1993)
128. O. Schenk, M. Bollhofer, R.A. Romer, SIAM J. Sci. Computing **28**, 963 (2006)
129. J. Dong, D.A. Drabold, Phys. Rev. Lett. **80**, 1928 (1998)
130. B.R. Djordjevic, M.F. Thorpe, F. Wooten, Phys. Rev. B **52**, 5685 (1995)
131. T.A. Abtew, M. Zhang, D.A. Drabold, Phys. Rev. B **76**, 045212 (2007)
132. Y. Pan, F. Inam, M. Zhang, D.A. Drabold, Phys. Rev. Lett. **100**, 206403 (2008)
133. Y. Pan, M. Zhang, D.A. Drabold, J. Non. Cryst. Sol. **354**, 3480 (2008)
134. F. Urbach, Phys. Rev. **92**, 1324 (1953)
135. H. Aoki, J. Phys. C-Solid State Physics **16**, L205 (1983)
136. J.J. Ludlam, S.N. Taraskin, S.R. Elliott, D.A. Drabold, J. Phys. Cond. Matter **17**, L321 (2005)
137. G.H. Wannier, Phys. Rev. **52**, 191 (1937)
138. E. Prodan, W. Kohn, Proc. Nat. Acad. Sci. **102**, 11635 (2005)
139. L. Pauling, *The Nature of the Chemical Bond* 3th edn. (Cornell University Press, Ithaca, 1960)
140. N. Marzari, D. Vanderbilt, Phys. Rev. B **56**, 12847 (1997)
141. S.F. Boys, Rev. Mod. Phys. **32**, 296 (1960)
142. U. Stephan, R.M. Martin, D.A. Drabold, Phys. Rev. B **62**, 6885 (2000)
143. P.L. Silvestrelli et al., Solid State Comm. **107**, 7 (1998)
144. U. Stephan, D.A. Drabold, Phys. Rev. B **57**, 6391 (1998)
145. W. Kohn, Phys. Rev. **115**, 809 (1959)
146. X. Zhang, D.A. Drabold, Phys. Rev. B **63**, 233109 (2001)
147. L. He, D. Vanderbilt, Phys. Rev. Lett. **86**, 5341 (2001)
148. S.N. Taraskin, D.A. Drabold, S.R. Elliott, Phys. Rev. Lett. **88**, 196405 (2002)
149. J. Ziman, *Models of Disorder: The theoretical physics of homogeneously disordered systems* (Cambridge University Press, Cambridge, 1979), pp. 456–457